Interaction between tensile fractures under varying orientations in Indiana Limestone

Bachelor Thesis

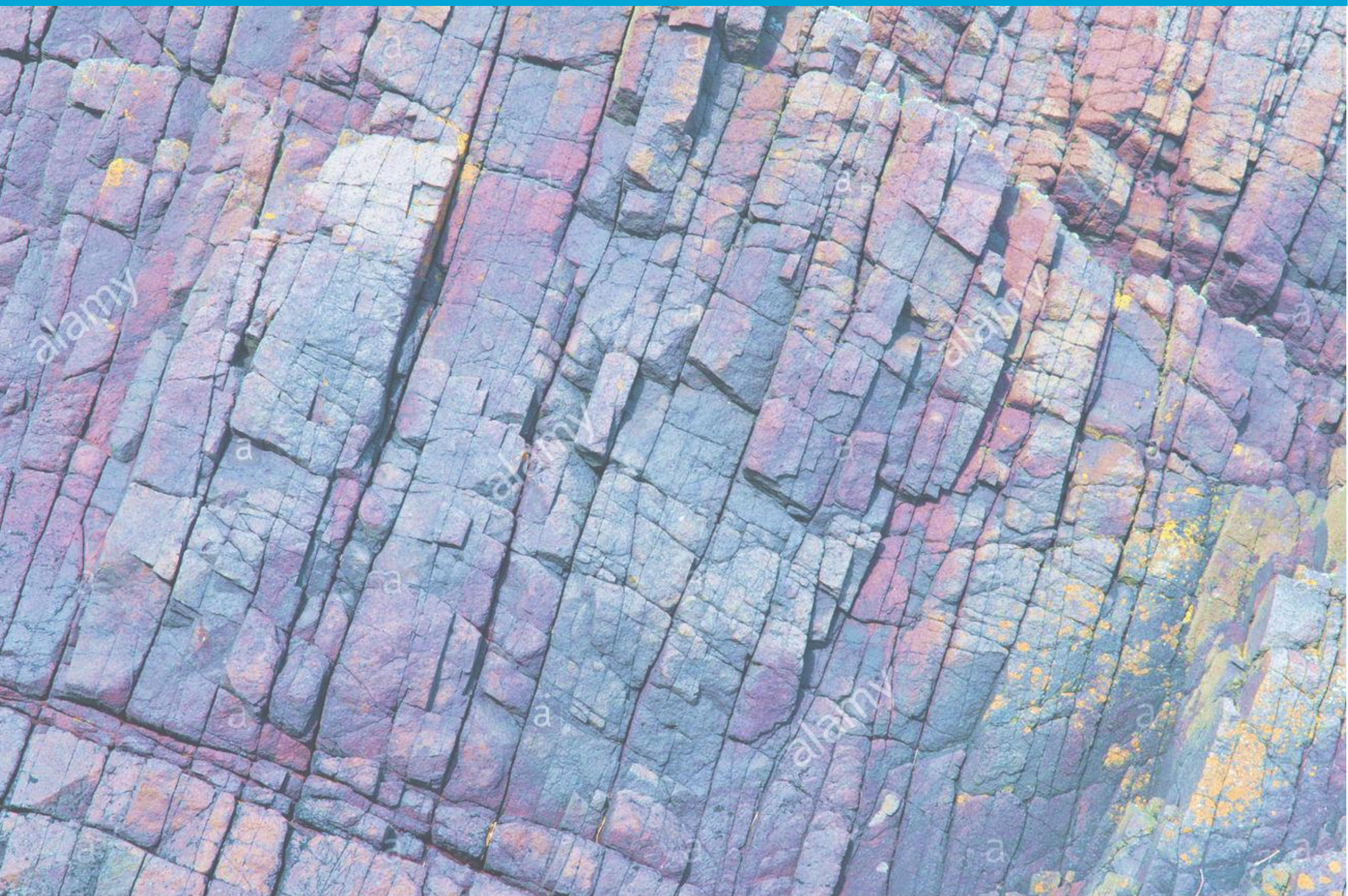

TU Delft

Friso ter Steege

-Blank page-

Bachelor Thesis

Interaction between tensile fractures under varying orientations in Indiana Limestone

By

Friso ter Steege

Bachelor of Science

In Applied Earth Sciences

At the Delft University of Technology

To be defended publicly on 9/7/19

Supervisors: Auke Barnhoorn; Dominque Ngan-Tillard; Anne Pluymakers

-Blank page-

1 Abstract

The interaction between fractures and the associated effects are studied in fields like geothermal engineering, seismology, volcanology and geo-engineering. Fractures can massively influence the permeability and porosity in a rock formation, reducing resistance to flow. However, to improve permeability, multiple fractures must connect to each other. Therefore, it is important to understand the effects of a stress field under varying orientations and how it influences new and existing fractures. Brazilian disc tests were filmed and performed on 18 Indiana limestone samples, after which 13 samples were fractured a second time under orientations varying from 20° to 90°. Afterwards, video footage of the tests was used to study fracture propagation and fracture roughness. Analysis of the results showed that four distinct types of fracture behaviour occurred. Each type was generally displayed between certain angles. Case 1, under 30° shows reactivation of the original fracture. Case 2, between 30 and 45°, shows largely reactivation of the primary fracture but new secondary fractures towards the ends of the sample. Case 3, between 45 and 60°, shows the primary fracture closing and formation of secondary fractures near the centre of the disk. Case 4, from 60° onwards, shows the primary fracture close completely while a new fracture forms perpendicular and independent of the first. The results imply that initiating a stress field in a certain orientation has differing consequences. A stress field more parallel towards the original fracture causes reactivation of the fracture, without much impact on the permeability. However, a stress field initiated perpendicular to the primary fracture causes a new fracture to form, independent of and straight through the primary fracture. This is likely to increase permeability and therefore reduce resistance to flow.

-Blank page-

2 Contents

1 Abstract 1
2 Contents 3
3 Acknowledgements 6
4 Introduction 7
4.1 Introduction 7
4.2 Indiana Limestone 8
4.3 Brazilian Disc Test – Theory 9
4.4 Brazilian Test - Setup 11
5 Materials & Methods 13
5.1 Dimensions and weight 13
5.2 Porosity measurements 14
5.3 Density & porosity comparison 15
5.4 Primary fractures & determining tensile strength 17
5.5 Secondary fractures 17
5.6 Fracture roughness 19
6 Results 20
6.1 Primary fractures 20
6.1.1 Fracture propagation 20
6.1.2 Stress-strain curves 20
6.1.3 Table 21
6.2 Secondary fractures 22
6.2.1 Fracture propagation 22
6.2.2 Stress-strain curves 26
6.2.3 Table 28
6.3 Fracture roughness 29
7 Discussion 30
7.1 Primary fractures 30
7.1.1 Result discussion 30
7.1.2 Comparison with other research 31
7.2 Secondary fractures 32
7.2.1 Result discussion 32
7.2.2 Zones 35
7.2.3 Fracture roughness 36

8 Conclusion 38
9 References 39

List of Tables

Table 1: First set of measurements performed on samples 13
Table 2: Pycnometer measurement results 14
Table 3: Secondary fracture orientations and samples 18
Table 4: Tensile strength for samples 21
Table 5: Results from secondary fracture tests 28
Table 6: Fracture roughness results 29
Table 7: Data for comparison 31
Table 8: Each sample and its behaviour 35
Table 9: Suggested fracture zones and typical behaviour 36

List of figures

Figure 1: Empire State Building. From History.com 8
Figure 2: Indiana Limestone sample 8
Figure 3: Common loading platen setups: a) flat plates, b) flat plates with cushion, c) flat plates with diameter rods and d) curved loading jaws. From: Perras & Diederich (2014) 9
Figure 4: Brazilian test with uniform load distributed over finite arcs. From: Li & Wong (2012) 10
Figure 5: Brazilian test setup 11
Figure 6: Closeup of sample in jaws. From Kourkoulis et al. (2013) 11
Figure 7: Examples of plots. From Riera et al. (2014) 12
Figure 8: Histogram of measured porosities 15
Figure 9: Expected porosity vs. measured porosity, with difference shown in yellow 15
Figure 10: Density against expected porosity, with fitted line and equation 16
Figure 11: Density against measured porosity, with fitted line and equation 16
Figure 12: Rotating the sample 17
Figure 13: Imported fracture image 19
Figure 14: Fracture converted into points 19
Figure 15: Sample 7 before, at the start, and at the end of fracturing 20
Figure 16: Stress vs. strain curves for first batch 20
Figure 17: 20° - sample 13 22
Figure 18: 30° - sample 4 22
Figure 19: 30° - sample 9 23
Figure 20: 35° - sample 11 23
Figure 21: 37.5° - sample 16 23
Figure 22: 40° - sample 6 24
Figure 23: 45° - sample 12 24
Figure 24: 45° - sample 14 24
Figure 25: 50° - sample 1 25
Figure 26: 50° - sample 7 25
Figure 27: 60° - sample 15 25
Figure 28: 60° - sample 20 25

Figure 29: 90° - sample 3 26
Figure 30: Stress-strain curves (20°-37.5°) 27
Figure 31: Stress-strain curves (40°-50°) 27
Figure 32: Stress-strain curves (60°-90°) 28
Figure 33: Bar chart of primary and secondary fracture roughness 29
Figure 34: Tensile stress distribution in sample. Red is highest. From: Li & Wong (2012) 30
Figure 35: Shear failures illustration 30
Figure 36: Histogram of tensile strength 30
Figure 37: Tensile strength comparison. Data from: Nazir et al. (2013), Schmidt (1976), Rinehart et al. (2015), Mellow & Hawkes (1971) and Baykasoğlu et al. (2008). 31
Figure 38: Clockwise from top left: Case 1 (sample 13); Case 2 (sample 9); Case 3 (sample 6); Case 4 (sample 7) 33
Figure 39: Close-up of sample 16 33
Figure 40: Stress-strain curves examples for each case 34
Figure 41: Histogram of secondary fracture tests 34
Figure 42: Stress against angle plot 36
Figure 43: Secondary fracture at 40° 37
Figure 44: Forced fracture 37

3 Acknowledgements

I would like to thank Auke, Dominque and Anne for their advice and investment into this project. Furthermore, the tests performed in the laboratory could not have happened without the help of Wim and Marc.

I wish Anne the best of luck with her ongoing research.

4 Introduction

4.1 Introduction

The interaction between multiple fractures is an important aspect in several fields. In geothermal applications, connected fractures can drastically improve permeability and flowrates in a reservoir. In seismology, fractures influence the propagation of waves and must be accounted for when mapping beneath the surface. Furthermore, reactivation of old fractures can cause earthquakes, which can be predicted with seismology analysis. Volcanologists also study the flow of magma and lava, which may flow through fracture systems deep underground. In geo-engineering fracture interaction matters because fractures can vastly decrease the strength of a rock. Therefore, understanding how multiple fractures interact with each other under differing stress fields is desirable in these fields.

This thesis investigates the interaction between tensile fractures. Fractures in rocks can have enormous effects on the strength, but also permeability and porosity of a rock (Einstein & Dershowitz, 1990). Therefore, understanding how these fractures originate and how they can be influenced is an important factor in multiple disciplines such as geo-engineering and hydraulic fracturing (Daneshy, 2010).

Fractures are present in many rock formations and are influenced by the orientation of the stress field. Old fractures may close while new fractures originate at the same time. Fracturing strongly increases the permeability of a rock by reducing the resistance to flow (Daneshy, 2010). However, if an old fracture compacts completely during this process, this effect may be diminished. Therefore, it is important to understand how fractures interact with each other, and how they propagate, under different orientations.

The Brazilian disc test is performed on 18 samples to induce a fracture. Thereafter, samples are fractured again under different orientations with the aim of finding a relation between the fracture propagation and the orientation. Furthermore, in order to study how the fracture path is influenced by a variation in the stress orientation, the fracture roughness is examined.

By studying and analysing these tests, an attempt is made to answer the following research question:

"How do primary fractures and secondary fractures interact under different angles during a Brazilian Disc test?"

4.2 Indiana Limestone

Indiana Limestone was originally used as a construction material, beginning in the 18th century (Selvadurai, 2010). In the latter part of the 19th century, Indiana Limestone was used in most governmental projects due to its appearance. However, the use of the stone as a building material is much more widespread. The Empire State building in New York is clad in Indiana Limestone (Powell, 2004), shown in Figure 1 (Andrews, 2018).

Figure 1: Empire State Building. From History.com

The samples studied in this thesis originate from the Salem Formation in Indiana, United States. This formation was formed in a shallow inland sea during the Mississippian period (Selvadurai, 2010). The rock is a grainstone formed from fossil fragments and cemented by calcite. The Indiana limestone consists almost entirely (>97%) out of calcite (Powell, 2004). Indiana limestone is a freestone, which means that it has no preferential direction of splitting, thus making it ideal for the purposes of the tests to be conducted in this thesis. This is particularly caused by the relative homogeneity of the rock (Selvadurai, 2010).

The specimens used for the tests performed in this thesis were cut from a block of Indiana Limestone. Cylinders with a diameter of about 30 mm were extracted from the block, after which the samples were cut to a thickness of half the diameter.

Figure 2: Indiana Limestone sample

Due to the absence of bedding in the samples, the effect of bedding can be considered negligible for the tests performed during this study.

4.3 Brazilian Disc Test – Theory

The Brazilian Disc Test is an indirect, simple test method to measure the tensile strength of brittle material, such as rocks. During the test, a thin, circular disc is diametrically compressed to failure (Li & Wong, 2012). This compression induces tensile stresses horizontally. The indirect tensile strength is calculated based on the assumption that the failure occurs at the place of maximum tensile stress, which is at the centre of the specimen (Li & Wong, 2012). According to Li & Wong and Perras & Diederich (2014), the formula used for calculating the tensile strength is:

$$\sigma_t = \frac{2P}{\pi D t} = 0.636\frac{P}{Dt} \qquad \text{(Eq. 1)}$$

Where P is the load at failure (in Newton), D is the diameter of the test specimen (mm) and t is the thickness of the disk (mm) (Li & Wong, 2012).

The International Society for Rock Mechanics standard suggests a curved set of jaws, with a radius of 1.5 times the disk radius for use in the test (Perras & Diederichs, 2014). However, there are multiple setups that are commonly used. These are shown in Figure 3.

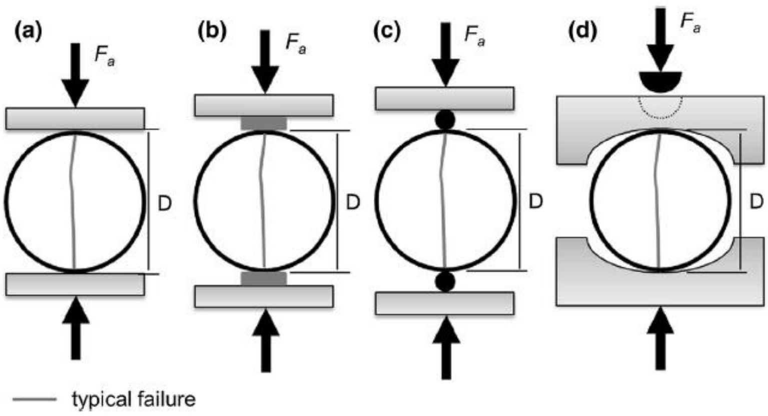

Figure 3: Common loading platen setups: a) flat plates, b) flat plates with cushion, c) flat plates with diameter rods and d) curved loading jaws. From: Perras & Diederich (2014)

The Brazilian disc test makes use of some assumptions. First, the frictional stresses between the plates and sample are neglected. Furthermore, the failure of a specimen is assumed to follow the Griffith criterion, and "the intermediate principal stress is assumed to have no influence of the fracture" (Li & Wong, 2012). The final, most important assumption is that the material of the rock is regarded as homogeneous, isotropic and linearly elastic before failure (Mellor & Hawkes, 1971). Because of this, Indiana limestone is particularly suitable to be used during the Brazilian tests.

For the case of a load distributed over finite arcs, such as 2α, a complete stress solution along the load diameter exists. This is illustrated in Figure 4, while the solutions are presented in Equations 2 and 3 (Li & Wong, 2012).

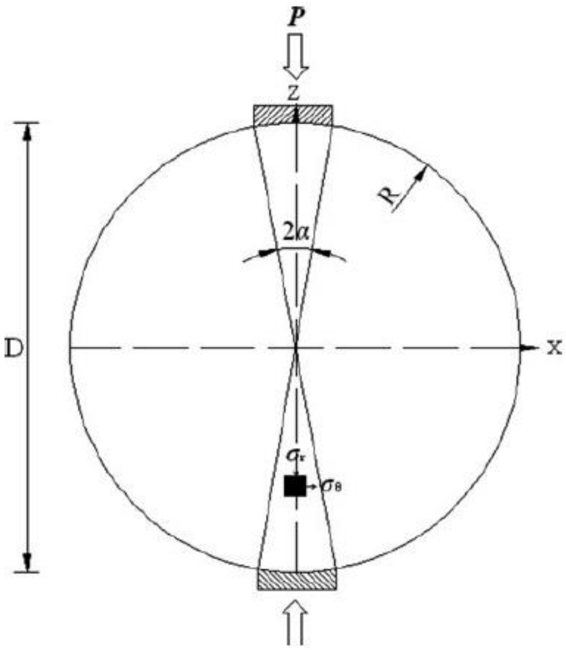

Figure 4: Brazilian test with uniform load distributed over finite arcs. From: Li & Wong (2012)

$$\sigma_1 = +\frac{P}{\pi R t \alpha}\left\{\frac{\left[1-\left(\frac{r}{R}\right)^2\right] sin2\alpha}{\left[1-2\left(\frac{r}{R}\right)^2 cos2\alpha + \left(\frac{r}{R}\right)^4\right]} - \tan^{-1}\left[\frac{1+\left(\frac{r}{R}\right)^2}{1-\left(\frac{r}{R}\right)^2} tan\alpha\right]\right\} \quad \text{(Eq. 2)}$$

$$\sigma_3 = -\frac{P}{\pi R t \alpha}\left\{\frac{\left[1-\left(\frac{r}{R}\right)^2\right] sin2\alpha}{\left[1-2\left(\frac{r}{R}\right)^2 cos2\alpha + \left(\frac{r}{R}\right)^4\right]} + \tan^{-1}\left[\frac{1+\left(\frac{r}{R}\right)^2}{1-\left(\frac{r}{R}\right)^2} tan\alpha\right]\right\} \quad \text{(Eq. 3)}$$

Where P is the applied load, R the radius of the disc, 2α the angular distance over which P is assumed to be distributed radially (which is mostly equal or smaller than 15°). Furthermore, t is the thickness of the disc and r is the distance from the centre of the specimen. The tensile stress is noted as positive (Li & Wong, 2012).

Li & Wong (2012) and Perras & Diederich (2014) note that these equations can be simplified in accordance to the Griffith criterion. According to their paper, only a 2% error is introduced when using these simplified equations for σ_θ. The equations are as follows:

$$\sigma_1 = +\frac{P}{\pi R t \alpha}\left\{\frac{sin2\alpha}{\alpha} - 1\right\} \approx +\frac{P}{\pi R t} \quad \text{(Eq. 4)}$$

$$\sigma_3 = -\frac{P}{\pi R t \alpha}\left\{\frac{sin2\alpha}{\alpha} + 1\right\} \approx -\frac{3P}{\pi R t} \quad \text{(Eq. 5)}$$

From: Li & Wong (2012)

4.4 Brazilian Test - Setup

The setup of the Brazilian test as performed during the tests is shown in Figure 5. The load cell is located at the very bottom. On top of the load cell are several plates and cylinders. These are in place to allow for the relatively small sample to be tested. The sample, encompassed by the jaws, is located on top of the plates and cylinders. A half ball bearing is situated at the top of the upper jaw, ensuring that the pressure is exerted at the vertical centreline of the specimen. At the very top of the setup the sensor can be seen. This sensor measures the amount of force exerted on it, and therefore on the sample. Furthermore, two LVDT sensors, each attached to wires are shown in the picture. These sensors measure the displacement of the plates.

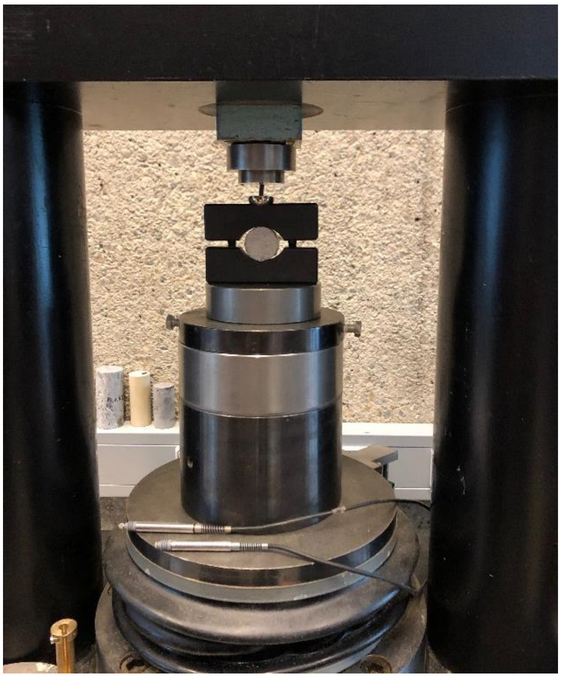

Figure 5: Brazilian test setup

A schematic close-up of the sample inside the jaws is shown in Figure 6 (Kourkoulis, Markides, & Chatzistergos, 2013). This figure shows how the specimen fits between the lower and upper jaw, which are kept in their spots using guide pins, located on either side of the jaws. An indent is clearly visible on the upper jaw. The half ball bearing fits in here, ensuring that the pressure exerted by the load cell is transferred correctly to the sample and sensor right above the ball bearing. Because the exerted pressure P (or σ_1) can be calculated from the force measured by the sensor, Equation 1 can be applied, allowing calculation of the tensile stress. The displacement sensors supply information on the vertical displacement of the plates. With this information known, it is possible to plot force or stress against displacement or time. This is illustrated in Figure 7 (Riera, Miguel, & Iturrioz, 2014).

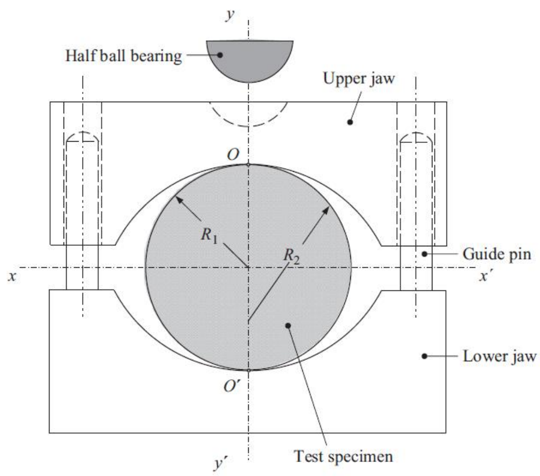

Figure 6: Closeup of sample in jaws. From Kourkoulis et al. (2013)

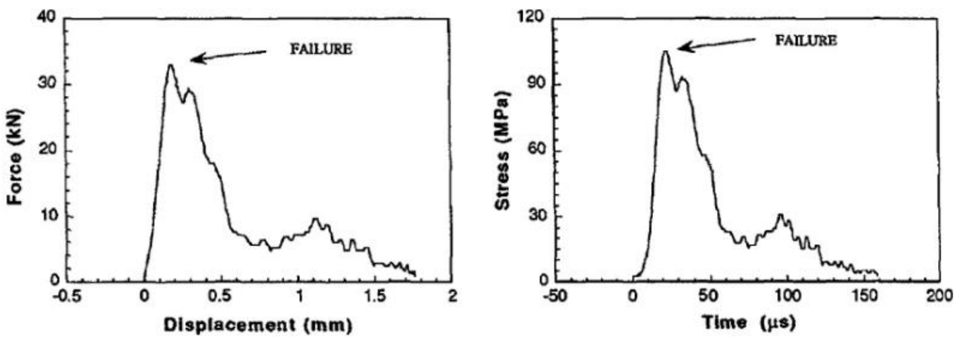

Figure 7: Examples of plots. From Riera et al. (2014)

Based on information shown like that in Figure 7, one can see the elastic phase but also predict when failure is about to happen. This can be used to an advantage, so that a sample does not completely split in half. This ensures that the sample can be used in further testing.

5 Materials & Methods

5.1 Dimensions and weight

A digital calliper was used to determine the dimensions of each sample, while a digital scale was used to weigh the samples. These measurements were each performed three times to reduce errors and inaccuracies. Noting that no outliers were present in these findings, a rounded average was taken and used for further calculations. The scale and calliper used had an error of ±0.005 g and ±0.005 mm, respectively. Combining equations 6-8 allowed the calculation of an expected porosity for each sample, shown in equation 9.

$$\phi = \frac{V_v}{V_b} \quad \text{(Eq. 6)}$$

$$m_{100} = V_b * \rho \quad \text{(Eq. 7)}$$

$$m_m = V_m * \rho \quad \text{(Eq. 8)}$$

$$\phi = \frac{V_b - (\frac{m_m * V_b}{m_{100}})}{V_b} \quad \text{(Eq. 9)}$$

Where ϕ is porosity, V_v is volume of voids, V_b is bulk volume, V_m is the matrix volume, m_{100} is the mass for 100% calcite, m_m is the measured mass and ρ is density. The measurements and calculation results are shown in Table 1.

Sample	Weight (g)	Length (mm)	Width (mm)	Bulk volume (cm³)	Density (g/cm³)	Expected Porosity
1	25.72	29.58	16.80	11.55	2.23	0.178
2	26.00	29.58	16.99	11.68	2.23	0.178
3	27.69	29.70	17.92	12.41	2.23	0.177
4	25.58	29.53	16.78	11.49	2.23	0.179
5	26.99	29.65	17.49	12.08	2.23	0.175
6	26.61	29.55	17.30	11.86	2.24	0.172
7	24.73	29.50	16.29	11.13	2.22	0.180
8	25.35	29.54	16.50	11.31	2.24	0.173
9	26.15	29.57	17.00	11.67	2.24	0.173
10	25.32	29.51	16.73	11.44	2.21	0.183
11	24.26	29.54	15.73	10.78	2.25	0.170
12	24.87	29.55	16.30	11.18	2.22	0.179
13	24.79	29.48	16.26	11.10	2.23	0.176
14	25.67	29.56	16.57	11.37	2.26	0.167
15	24.32	29.50	15.95	10.90	2.23	0.177
16	25.68	29.61	16.75	11.53	2.23	0.178
17	24.82	29.58	16.11	11.07	2.24	0.173
18	24.82	29.42	16.31	11.09	2.24	0.174
19	24.09	29.55	15.73	10.79	2.23	0.176
20	24.29	29.51	15.85	10.84	2.24	0.173
21	25.06	29.61	16.30	11.22	2.23	0.176
22	23.59	29.54	15.44	10.58	2.23	0.177

Table 1: First set of measurements performed on samples

5.2 Porosity measurements

A pycnometer calculates the matrix volume by injecting gas in a chamber with a known volume. With the matrix volume, bulk volume and mass known, equation 10 can be used to calculate the porosity. The results are shown in Table 2.

$$\phi = \frac{V_b - V_m}{V_b} \quad \text{(Eq. 10)}$$

Sample	Matrix volume (cm³)	Matrix density (g/cm³)	Porosity
1	9.3150	2.7611	0.193
2	9.4550	2.7499	0.190
3	10.0967	2.7425	0.187
4	9.3140	2.7464	0.190
5	9.8449	2.7415	0.185
6	9.6151	2.7675	0.190
7	8.9535	2.7621	0.196
8	9.1872	2.7593	0.188
9	9.4839	2.7573	0.188
10	9.1557	2.7655	0.200
11	8.7960	2.7581	0.184
12	9.0184	2.7577	0.193
13	9.0047	2.7530	0.189
14	9.3511	2.7451	0.178
15	8.8348	2.7528	0.190
16	9.3198	2.7554	0.192
17	9.0372	2.7464	0.184
18	8.9858	2.7621	0.190
19	8.7155	2.7640	0.192
20	8.8256	2.7522	0.186
21	9.0925	2.7561	0.190
22	8.5286	2.7660	0.194

Table 2: Pycnometer measurement results

5.3 Density & porosity comparison

Figure 8 shows a histogram of the measured porosities. The porosity values lie relatively close together ranging from 17.8 to 20.0 %. These findings are in line with the expectations for a homogeneous rock. Furthermore, due to the low variability of porosity, no considerable impact from porosity on the fractures is expected.

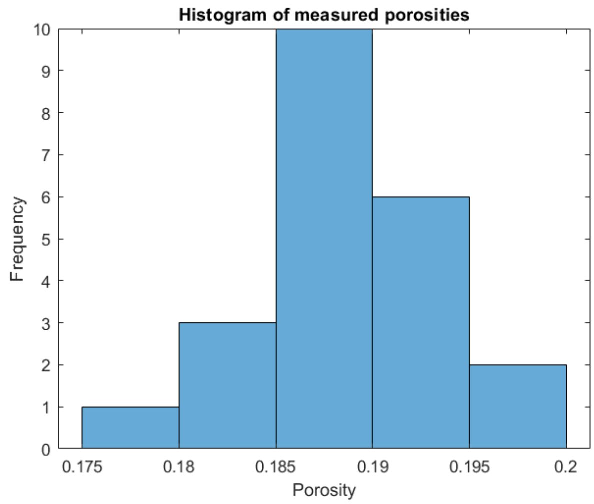

Figure 8: Histogram of measured porosities

Second, the expected porosities are plotted against the measured porosity values (Figure 9). Both sets of values clearly follow the same trend. The expected porosities are always lower, by an almost constant difference, shown in yellow. The expected porosities are consistently around 8 % lower than the measured values. Figure 9, especially the recognisable trend in both datasets, further indicates the homogeneity in the Indiana limestones.

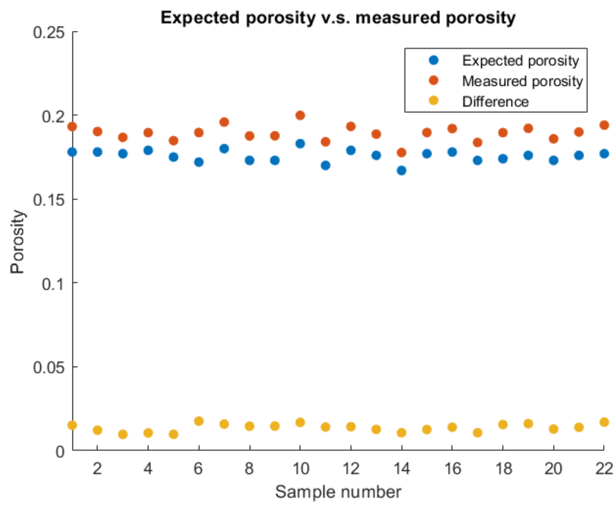

Figure 9: Expected porosity vs. measured porosity, with difference shown in yellow

Figure 10 plots the density against the expected porosity. A relation is described by the following equation:

$$y = -2.8x + 2.7 \qquad \text{(Eq. 11)}$$

In contrast to the expected porosities, the porosity values based on the pycnometer measurements do not depend on the density. Therefore, to find out if there is a relation between density and porosity, a similar fitted line should be seen in Figure 11.

Compared to Figure 10, the data points shown in Figure 11 do not indicate such a clear line. However, the cloud of points still allows for a very similar fitted line.

$$y = -1.9x + 2.6 \qquad \text{(Eq. 12)}$$

Although these equations differ slightly, they are similar enough to indicate a clear direct relation between the density and porosity of the Indiana limestone samples.

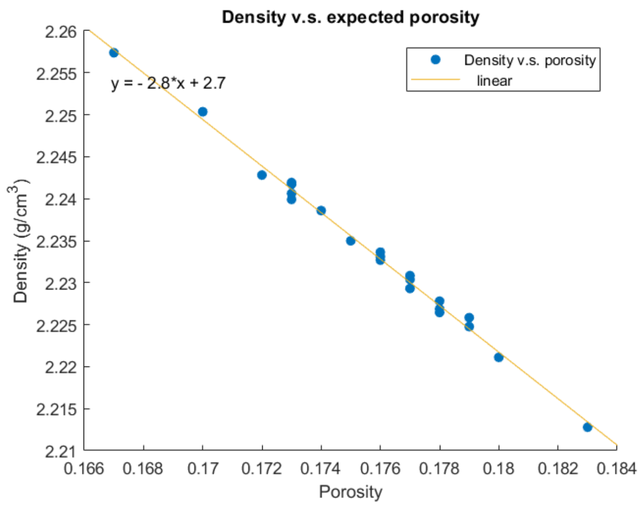

Figure 10: Density against expected porosity, with fitted line and equation

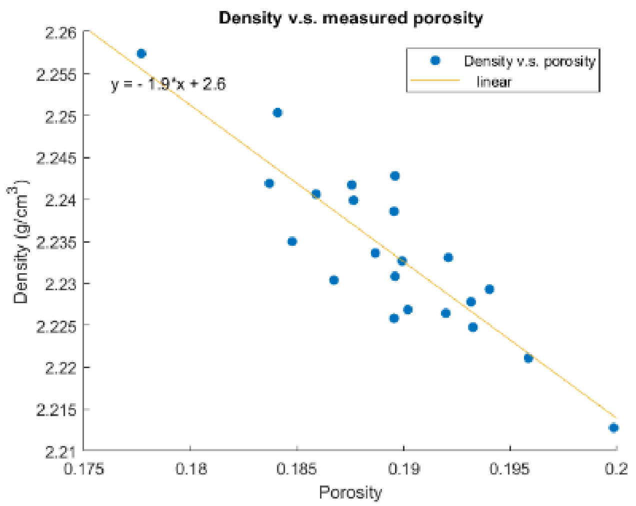

Figure 11: Density against measured porosity, with fitted line and equation

5.4 Primary fractures & determining tensile strength

In the laboratory, 18 samples were selected to be split. In order to prevent the samples to completely split, each disk was wrapped with duct tape. The added thickness and influence on fracture propagation was deemed negligible. Firstly, chipped samples were fractured in order to improve experience and accuracy with the machine for later tests. The remaining 4 samples were kept intact, as a backup for the rest of the project, or to undergo further testing if deemed necessary. The samples were filmed during testing. This allowed for closer analysation of the samples during their fracturing process

The computer software controlling the machine performed all tests using the same user settings, the most notable being the speed of movement of 1 micrometre per second. The force (in kN) and displacement (in mm) was used to calculate the stress and strain. The stress (in MPa) is calculated using Equation 1, while the strain is calculated using Equation 13.

$$\epsilon = \frac{dl}{L} \qquad \text{(Eq. 13)}$$

5.5 Secondary fractures

After the 18 samples had been split, the second stage of laboratory testing commenced. In this phase, the behaviour of secondary fractures was studied by varying the orientation between the primary fracture and the new stress field. The orientation was determined by using a degree circle on transparent paper, with steps of 5°. This is shown in Figure 12. The first batch of secondary fracture tests were done with orientations of 90°, 45°, 37.5°, 30° and 20°. It emerged that the most interesting range of values was around the 45° mark and therefore following experiments focused on this range.

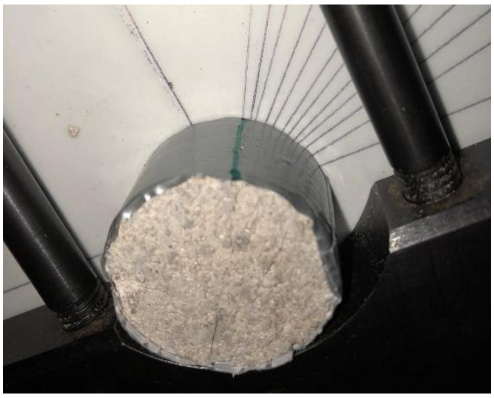

Figure 12: Rotating the sample

In order to study how the fractures interact with each other while the relative orientation varies, snapshots were made from the videos captured in the laboratory. The snapshots show the situation before the test, before failure and after failure.

The used samples and their orientations are shown in Table 3. Apart from the rotation, the tests were performed analogous to the primary fracture tests.

Orientation (°)	Sample
20	13
30	4
30	9
35	11
37.5	16
40	6
45	12
45	14
50	1
50	7
60	15
60	20
90	3

Table 3: Secondary fracture orientations and samples

5.6 Fracture roughness

As the primary and secondary fractures were formed under different circumstances, the fracture roughness was studied. The fracture roughness is usually defined as the root mean square error (RMS). For a qualitative analysis to be possible, a process was drawn up so that results could be reliably compared to each other. The fractures drawn in Section 6.2 were extracted, rotated clockwise into a horizontal position, then saved as a primary and secondary fracture image file (shown in Appendix IV). Then, a MATLAB script (Appendix V) imported the image file and detected the fracture, as shown in Figure 13. Thereafter, the detected line was converted into points, shown in Figure 14. Based on this data, a fitted line was calculated. From this fitted line, it was possible to determine the RMS error using Equation (14) and thus the fracture roughness.

$$x_{RMS} = \sqrt{\frac{1}{N}\sum_{n=1}^{N}|x_n|^2} \qquad \text{(Eq. 14)}$$

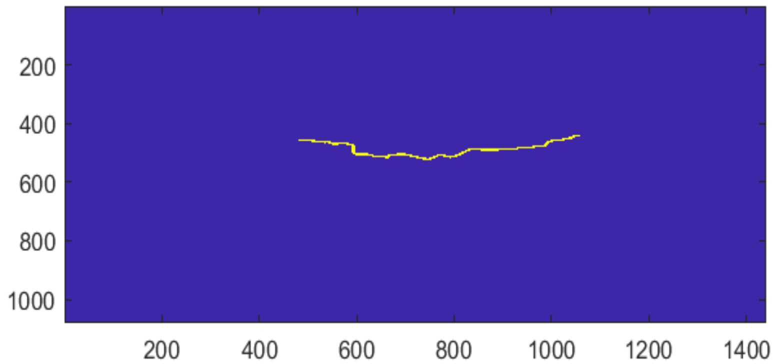

Figure 13: Imported fracture image

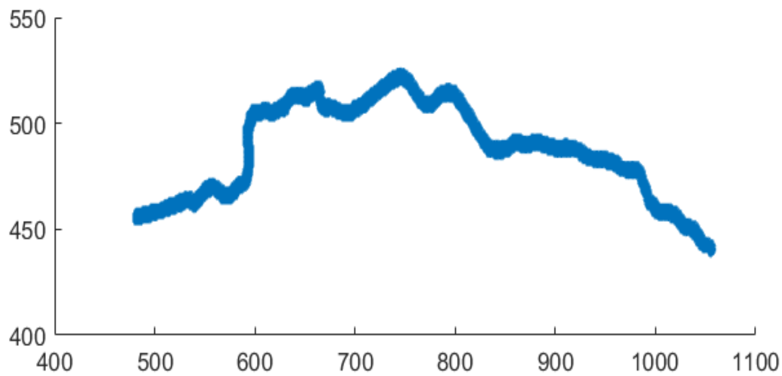

Figure 14: Fracture converted into points

6 Results

6.1 Primary fractures

6.1.1 Fracture propagation

Figure 15 shows the fracture propagation in sample 16. At the start of the test, no fracture is visible. Then, when the first cracks show up these are in the centre of the sample. At failure, those cracks propagate towards the ends of the sample. This was the case for all samples.

Figure 15: Sample 7 before, at the start, and at the end of fracturing

6.1.2 Stress-strain curves

Figure 16 shows the stress-strain curves for all 18 samples, until just after failure. Based on the information provided by Figure 16, the maximum tensile strength could be found. Stress-time plots are shown in Appendix I.

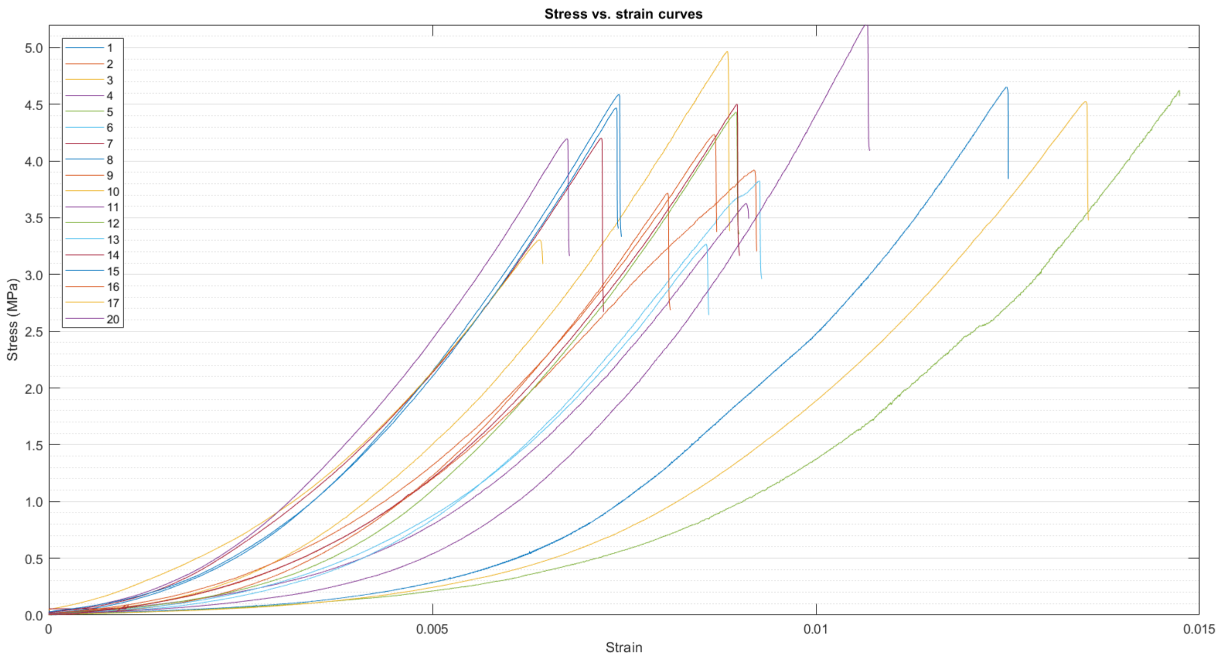

Figure 16: Stress vs. strain curves for first batch

6.1.3 Table

Table 4 depicts each sample with its associated tensile strength value. If a sample did not split cleanly, this is noted in the 3rd column of Table 4.

Sample	Tensile strength (MPa)	Notes
1	4.65	Small secondary fracture near one end
2	3.92	
3	4.97	
4	3.63	
5	4.62	Fracture splits around clast at one end
6	3.82	
7	4.20	
8	4.59	Secondary fracture near one end at ±45°
9	3.72	
10	3.30	
11	4.20	
12	4.43	
13	3.27	
14	4.50	
15	4.67	Secondary fracture near one end at ±30°
16	4.23	
17	4.52	Fracture splits in two from midpoint
20	5.21	Secondary fracture near one end at ±20°

Table 4: Tensile strength for samples

6.2 Secondary fractures

6.2.1 Fracture propagation

Figure 17 through Figure 29 show the process during the secondary fracture tests. To the left, the situation before the start of the test is depicted. The centre image shows the sample just before failure, while the rightmost picture depicts the situation after failure has occurred. The fractures have been accentuated for clarity. Black lines represent primary fractures while red lines accentuate secondary fractures. Unedited photos are in Appendix III.

Figure 17: 20° - sample 13

Figure 17 shows no closing of the fracture but clear sliding. This is most likely caused because the orientation of the fracture makes it impossible for a reasonable amount of friction to emerge. When the jaws exert pressure on the sample, the top half simply slides downward. Figure 30 shows no indents in the stress-strain curve, indicating that sliding occurred gradually, supporting the idea that friction was not a major factor in this test.

Figure 18: 30° - sample 4

Although Figure 18 also depicts sliding between the two halves, the stress strain curve shown in Figure 30 indicates clear indents in its data. These dents may specify grains chipping off the sample or sliding movement. Based on the pictures, these indents most likely represent the moments where sliding occurred. In contrast to sample 13, the sliding in this case did not happen continuously, again illustrated by the dents on the stress-strain curve. The images also show that there is some compaction of the fracture due to the compression. Therefore, it is likely that in this case there was enough friction between the two halves to accommodate this behaviour.

Figure 19: 30° - sample 9

Figure 19 shows a different sample tested with the same orientation. In this case, no compaction of the original fracture is seen, but new secondary fractures are formed after failure. It appears that the new fracture path used mostly the pre-existing crack in the centre and split off towards the ends of the sample. No sliding is noticeable, so it is likely that enough friction existed to stop this from occurring.

Figure 20: 35° - sample 11

Figure 20 indicates that the original fracture completely disappears due to the compression of the sample. After failure, a new fracture forms, almost completely different from the original fracture.

Figure 21: 37.5° - sample 16

The difference between Figure 20 and Figure 21 is quite hefty for tests performed at roughly the same orientation. Although the fracture compacts in both tests, the fracture in Figure 20 closes completely and becomes invisible. After failure, a new crack is formed which almost fully disregards the original fracture. However, in Figure 21, secondary fractures only form in the lower part of the sample, while mostly using the original crack.

Figure 22: 40° - sample 6

Figure 22, tested at 40°, has been tested with a similar orientation. However, in this case, the original fracture does not seem to close. After failure, a new secondary fracture develops from the centre of the sample, using a small part of the pre-existing fracture. Even though the tests shown in Figure 20 through Figure 22 were performed under similar conditions, the results differed greatly. This is most likely caused by the heterogeneity of the samples. As has been seen in primary fracture testing, a clast or fossil can disturb the natural growth of a fracture. Furthermore, these fractures propagate in a 3rd dimension; left unseen during this study.

Figure 23: 45° - sample 12

Figure 24: 45° - sample 14

Like Figure 22, Figure *23* depicts sample 12 under a 45° orientation. The original crack compacts somewhat and after failure a secondary fracture emerges, using the centre part of the old fracture. Figure 24 strictly resembles Figure 20, where the pre-existing fracture closes completely and a new fracture forms after failure, completely independent from the original crack. It appears that if the original fracture closes fully, the secondary fracture goes straight through. If the original crack is not fully closed, the fracture seems to go through part of the old fracture. Since fractures follow the path of least resistance, it is logical that part of the old fracture is used if it still open after compression, as the cracks open in the centre of the sample.

Figure 25: 50° - sample 1

Figure 26: 50° - sample 7

The two tests performed at 50° closely resemble the samples tested at 45°. The first test at 50° (Figure 25) is much alike Figure 22 and Figure 23. Again, the fracture compacts slightly, and a new fracture forms using the centre of the pre-existing crack. The second test, depicted in Figure 26 is comparable to Figure 24 and Figure 20, where the original crack completely disappears under pressure. Then, a secondary fracture is formed vertically, independent of the first. The variance in these results is likely explained by heterogeneity, a 3rd dimension but also errors in measurement.

Figure 27: 60° - sample 15

Figure 28: 60° - sample 20

Figure 29: 90° - sample 3

The three tests performed between 60 and 90° are shown in Figure 27 through Figure 29. In these cases, the original fracture closes fully and a secondary fracture forms independently of the first. It therefore appears that if the angle between the first and second fracture is large enough, the force exerted by the jaws is too large for the original crack to have any significant impact on the forming of a new fracture.

6.2.2 Stress-strain curves

Figure 30 through Figure 32 depict the stress-strain curves for the secondary fracture tests. Stress against time plots for some of the tests are illustrated in Appendix II.

Figure 30 depicts tests with the orientations between 20° and 30°. It shows that the lower angles generally have a lower tensile strength, with the exceptions being sample 4 and 16. This graph contains the three lowest maximum tensile strength values of the secondary fracture tests.

Figure 31 shows the results for the range between 40° and 50°. Although there is variance in the maximum tensile strengths, the differences are much less severe than in Figure 30. This indicates that the tests shown in this graph more alike than those shown in Figure 30.

The tests for 60° and 90° are illustrated in Figure 32. These tests have a similar maximum tensile stress and also show the same behaviour described in Section 6.2.1. The tensile strengths are comparable to the two highest values in Figure 31.

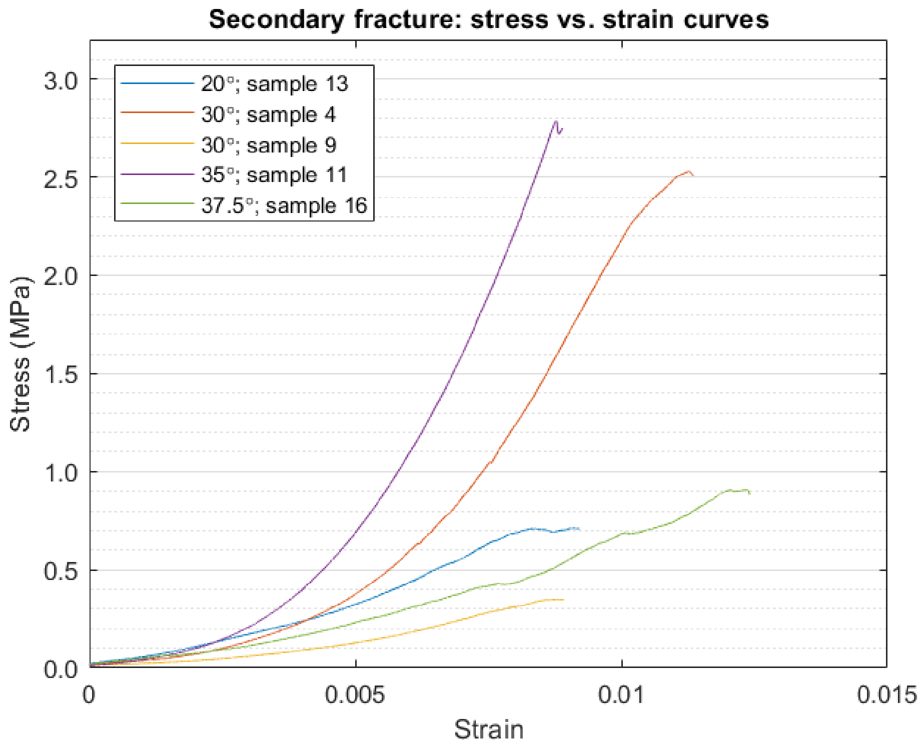

Figure 30: Stress-strain curves (20°-37.5°)

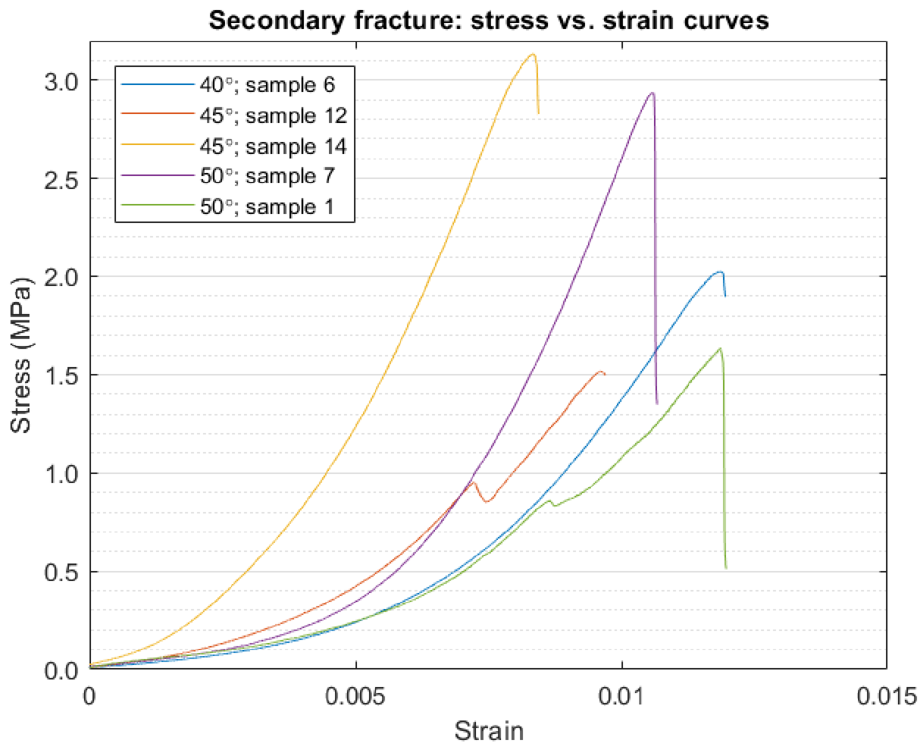

Figure 31: Stress-strain curves (40°-50°)

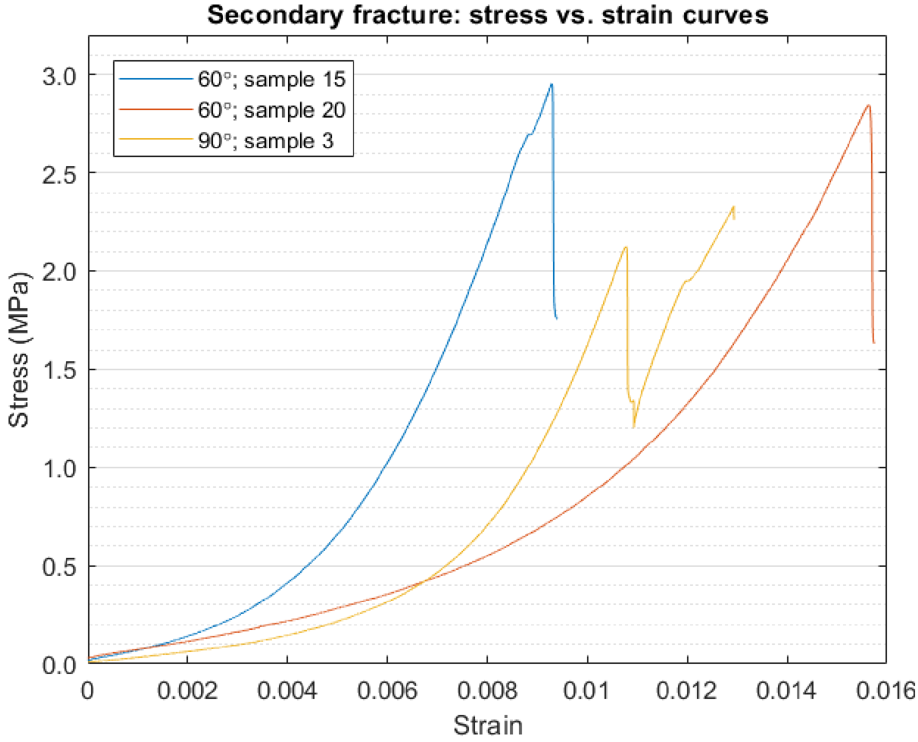

Figure 32: Stress-strain curves (60°-90°)

6.2.3 Table

The observations and calculations from sections 6.2.1 and 6.2.2 are presented in Table 5. The table shows a clear trend from lower to higher tensile strength as the relative orientation increases. Furthermore, the closing of the original fracture is more likely with a larger orientation. Partial use of the original fracture is more likely at lower relative orientations. Lastly, at shallower angles, sliding occurs more frequently.

Relative orientation	Sample	Tensile strength (MPa)	Primary fracture closes	New fracture(s)	Uses (part of) original fracture	Sliding seen on snapshots
20°	13	0.71	No	No	Yes	Yes
30°	4	2.53	Slightly	Yes	Yes	Yes
30°	9	0.35	No	Yes	Yes	No
35°	11	2.78	Yes	Yes	No	No
37.5°	16	0.91	Slightly	Yes	Yes	Yes
40°	6	2.02	No	Yes	Yes	No
45°	12	1.52	Slightly	Yes	Yes	No
45°	14	3.13	Yes	Yes	No	No
50°	1	1.64	Slightly	Yes	Yes	No
50°	7	2.93	Yes	Yes	No	No
60°	15	2.95	Yes	Yes	No	No
60°	20	2.84	Yes	Yes	No	No
90°	3	2.33	Yes	Yes	No	No

Table 5: Results from secondary fracture tests

6.3 Fracture roughness

The MATLAB script (Appendix V) calculated the roughness of the fracture images (Appendix IV) provided to the program. It should be noted that this was done only for cases where a second fracture appeared; therefore, this excludes samples 4 and 13. The results are presented in Table 6.

Angle	Sample	Roughness 1st fracture	Roughness 2nd fracture
30	9	22.438	41.555
35	11	22.960	37.647
37.5	16	8.654	11.556
40	6	7.314	81.398
45	12	18.260	11.693
45	14	9.334	40.709
50	1	20.141	15.663
50	7	16.839	14.722
60	15	23.787	13.372
60	20	24.000	27.257
90	3	33.360	27.834

Table 6: Fracture roughness results

The information from Table 6 is displayed in Figure 33. It depicts the fracture roughness of each test. The blue bars represent the fracture roughness of the original fracture, while the orange bars refer to the secondary fracture. Generally, the chart seems to indicate a relatively higher secondary fracture roughness under 50°, and a relatively lower secondary fracture roughness above 50°. However, tests at 45° and 60° do not conform to this trend. Furthermore, the secondary fracture roughness at 40° is strikingly high, which may indicate an unreliable data point.

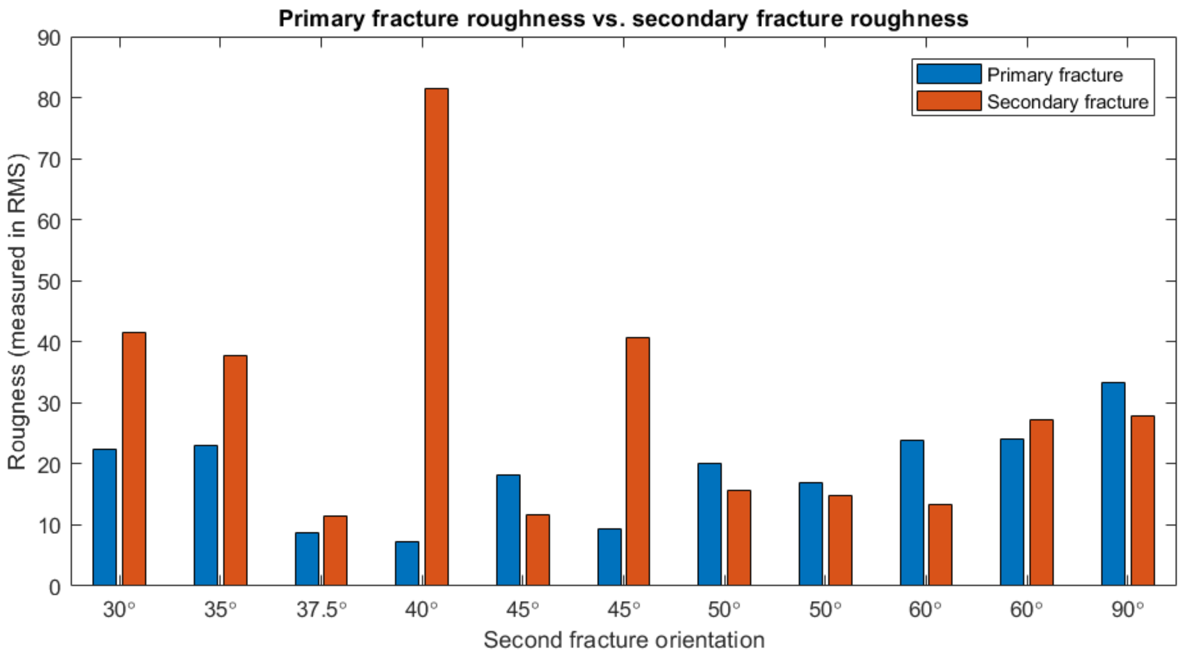

Figure 33: Bar chart of primary and secondary fracture roughness

7 Discussion

7.1 Primary fractures

7.1.1 Result discussion

As depicted in Figure 15, it appeared in all cases that the fractures emerged from the centre of the disk. This is explained by the distribution of the tensile stresses inside the sample. Using a computer model, Li & Wong (2012) illustrated the stresses inside the disk, as shown in Figure 34. This model evidently demonstrates that the tensile stresses are largest in the centre. Therefore, the fractures made during the laboratory work always started in the middle.

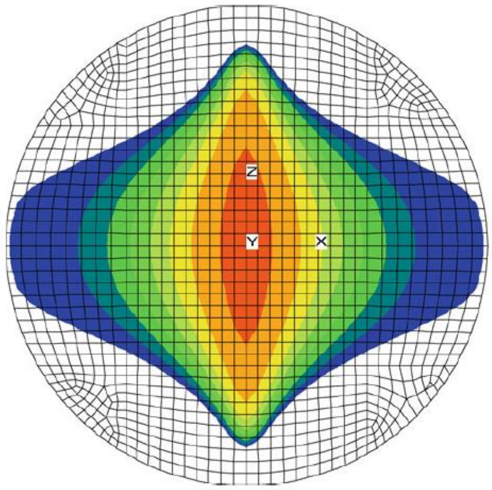

Figure 34: Tensile stress distribution in sample. Red is highest. From: Li & Wong (2012)

A second observation made during the primary fracture tests, as stated in Table 4, is that in some cases, the fracture did not split the sample cleanly. Notably towards the top and bottom of the samples, more smaller cracks were spotted. Examples of this can be found in Figure 22 and Figure 23. This behaviour is also discussed by Li & Wong (2012). As Figure 34 shows, the tensile stresses are also relatively high towards the top and bottom – where the force is exerted. The result of this is shown in Figure 35. These smaller fractures are the result of shear stress around the contact points with the jaws.

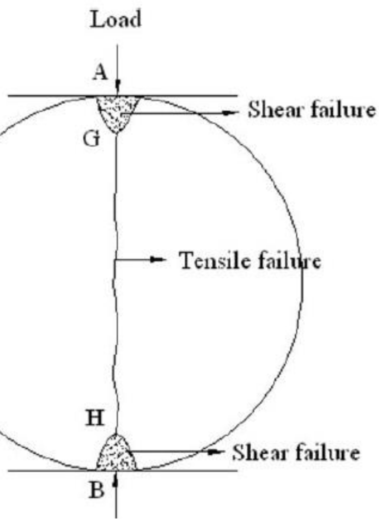

Figure 35: Shear failures illustration

However, these secondary fractures were not always caused by shear stress. The histogram (Figure 36) displays a normal distribution of values. Such a result is expected, but comparing the data from Figure 36 and Table 4 reveals an interesting connection. All samples with smaller secondary cracks have a tensile strength higher than 4.5 MPa. These make up the rightmost two bars of the histogram. As described by the notes and seen in some of the figures from Section 6.2.1, these are caused by the fracture having to move around a clast or fossil. This increases the energy needed for a full fracture to form – therefore inflating the tensile strength value. Although Indiana limestone is relatively homogeneous, these cases show that true homogeneity is merely an assumption.

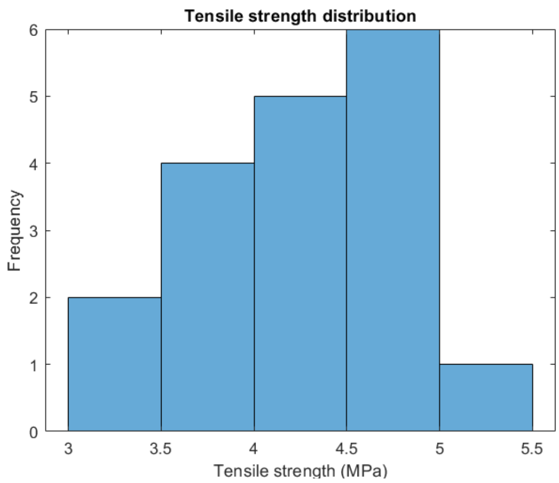

Figure 36: Histogram of tensile strength

Section 6.1.2 displays the stress-strain curves for the 18 samples that were fractured during the first laboratory tests. The graph shows most tests to fail around a stress of 4.0 MPa and a strain of 0.075 mm. Although there are a few tests with higher and lower values of stress and strain, this fits in the normal distribution. Figure 16 indicates that the tests have been performed rather consistently and it does not show any notable outliers.

7.1.2 Comparison with other research

In order to compare and evaluate the data found from the tested sample, several datasets were gathered from literature. From this data, a mean and standard deviation was calculated. The external data, together with the data from the laboratory work presented in this paper is shown in Table 7.

Data source	**Sample size**	**Mean**	**Standard deviation**	**Indiana Limestone**
Nazir et al. (2013)	20	7.15	2.59	No
Schmidt (1976)	6	5.38	0.41	Yes
Rinehart et al. (2015)	16	5.92	0.61	Yes
Mellow & Hawkes (1971)	60	6.00	0.38	Yes
Baykasoğlu et al. (2008)	118	3.80	2.50	No
Tested samples	18	4.24	0.54	Yes

Table 7: Data for comparison

This shows that a total of 138 non-Indiana limestone and 100 Indiana limestone samples were used for the creation of Figure 37, a total sample size of 238.

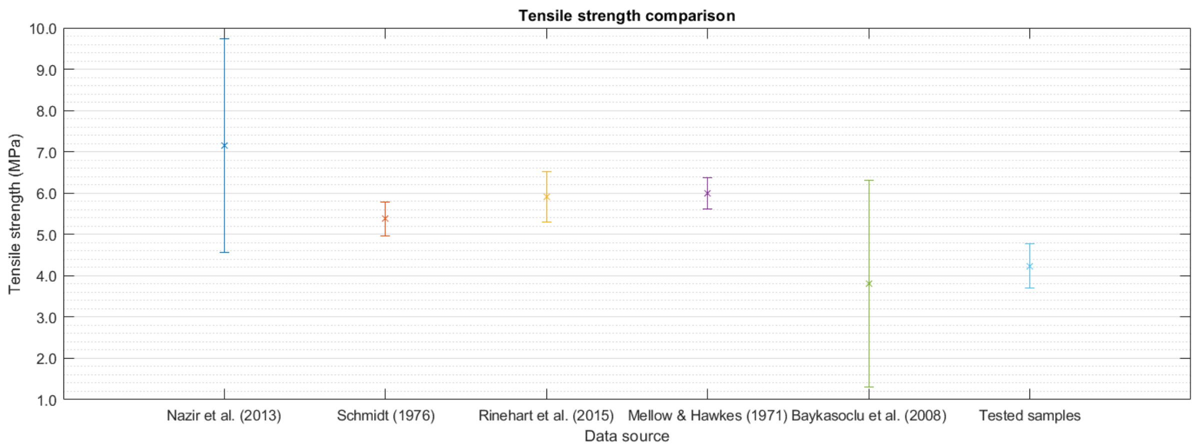

Figure 37: Tensile strength comparison. Data from: Nazir et al. (2013), Schmidt (1976), Rinehart et al. (2015), Mellow & Hawkes (1971) and Baykasoğlu et al. (2008).

As noted in Table 7, set 1 and 5 contain data for non-Indiana limestone samples, while sets 2-4 and 6 represent Indiana limestone. Immediately noticeable is the variability in non-Indiana limestones. The first dataset reports a mean value of 7.15 (Nazir, Momeni, Armaghani, & Amin, 2013), while the fifth paper found a mean of 3.8 (Baykasoğlu, Güllü, Çanakçı, & Özbakır, 2008). In stark contrast to these findings are the three independent papers by Schmidt, Rinehart et al. and Mellow & Hawkes. These datasets are all generated with Indiana Limestones, and although the sample sizes are relatively smaller, these three bars show a clear relation to each other. For a start, the mean values lie very close to each other (5.38, 5.92 and 6.00). Furthermore, the associated standard deviations are low. However, although Figure 37 shows that the external

Indiana limestone datasets have comparable mean and standard deviation values, the mean from the samples tested in this thesis is considerably lower. A surprising contrast is that the mean tensile stress is 4.24 MPa. Comparing this to the tensile strengths in Figure 37 indicates a significant difference. The values found in this report are lower than those presented in Figure 37. However, Schmidt (1976), of the sources for Figure 37, notes in his report: "*Tensile test results indicate a considerably higher tensile strength… than were reported by Hoagland et al. and Hardy et al.*" The values Schmidt referred to were 3.58 MPa and 3.52 MPa, respectively. These values are lower than those experimentally found in this report. However, he does not mention a possible difference in porosity or density between the studies.

A very likely cause of the discrepancy between mean values is the difference in porosity. Schmidt (1976) reports a porosity between 10-15%, while values in Rinehart et al. (2015) shows porosities to be around 15%. These are significantly lower than those presented here in Table 2. Although Mellor & Hawkes (1971) do not mention the porosity or density of the tested samples, it is likely that these are in the same range as Schmidt and Rinehart et al.

Therefore, the difference in the mean value is most likely caused by a difference in porosity. As the standard deviations of the external datasets agree completely with the samples tested in this report and the difference in mean is explained by different porosities, it appears that the findings are in line with what is known about Indiana limestone.

7.2 Secondary fractures

7.2.1 Result discussion

Fracture behaviour

Based on the results presented in Section 6.2 and the information from Table 5, it appears that the results can be categorised in four scenarios. First, the old fracture does not close, no new fracture forms and sliding occurs (Case 1 – Figure 38). Second, the pre-existing crack does not compact, but new fractures form at the ends of the sample, using a significant part of the primary fracture (Case 2 – Figure 38). Third, the primary fracture closes somewhat, and a secondary fracture occurs, using the centre part of the original fracture (Case 3 -Figure 38). Fourth, the original crack completely closes, and a secondary fracture emerges straight through, disregarding the old crack (Case 4 – Figure 38).

If the original fracture closes completely, such as in Case 4, it may be interesting to study how this influences the permeability of the rock. Many fractures in a rock do not necessarily improve the flow rate through a reservoir. For this to occur, fractures need to connect or intersect with other. In hydraulic fracturing, a second fracture may be induced to intersect and increase production rate. However, if the creation of the secondary fracture closes off the primary fracture, the positive effects may be negated. For a fracture to improve production "the hydraulic fracture should offer very little resistance to flow" (Daneshy, 2010). This happens if an old fracture is reopened, or a new intersecting fracture is formed. It is therefore interesting to investigate if the closed fracture also reduces its flow resistance. If this is the case, then the orientation of the stress field is a very important factor in determining the overall increase of production.

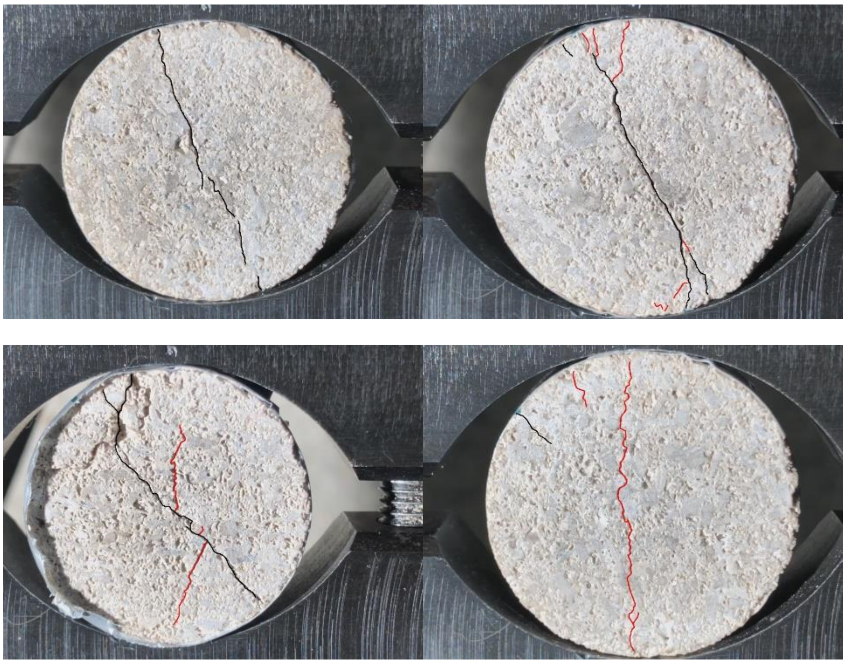

Figure 38: Clockwise from top left: Case 1 (sample 13); Case 2 (sample 9); Case 3 (sample 6); Case 4 (sample 7)

Stress-strain curves

The stress-strain curves displayed in Figure 30-Figure 32 generally agree with the discussion based on the pictures. In the cases where sliding occurred, at smaller angles, the tensile strength was significantly lower than the other samples (sample 13 & 16). Furthermore, the stress-strain curves of the samples that generated a secondary fracture, completely independent from the first, have generally higher tensile strength values (samples 3, 7, 11, 14, 15 & 20). This is likely because in these cases, the original fracture closes completely. This means that there is more energy needed to create a new fracture; leading to a higher tensile strength.

A notable outlier from the data shown in Figure 30 is sample 16 at an orientation of 37.5°. The tensile strength value is notably low. Upon closer inspection in Figure 39, it seems that some hairline fractures were present before the start of the secondary fracture test. Comparing these fractures to the picture after failure (Figure 21) it seems that the secondary fractures formed along those small pre-existing cracks. This has likely severely diminished the strength of the sample, explaining its unexpectedly low tensile strength value during the second test.

Figure 39: Close-up of sample 16

Figure 40 draws the stress-strain curves for each of the four cases. Although not enough data is available to draw any hard conclusions from the tests at lower angles (30° and under), case 1 would usually be expected to have a lower tensile strength than case 2, as only sliding occurs. This idea contradicts Figure 40, however. Case 4, the tests where the primary fracture closes, does consistently show higher tensile strength values than case 3.

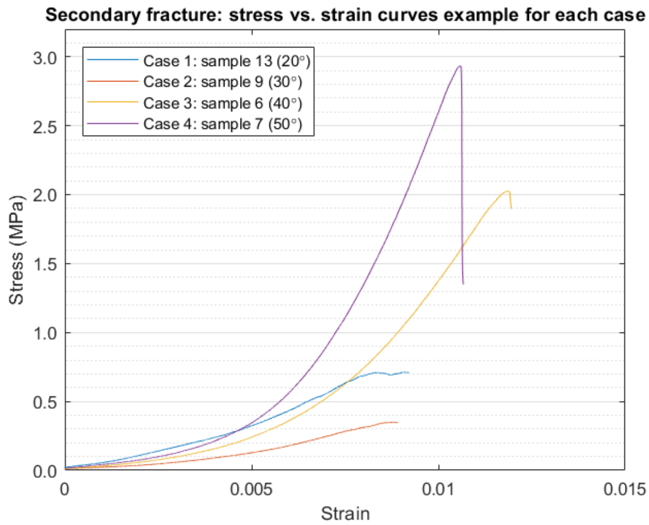

Figure 40: Stress-strain curves examples for each case

Figure 41 displays the distribution of the tensile stress values after the second laboratory tests. The histogram does not follow a smooth normal distribution such as in Figure 36. This is likely caused by the damages the samples incurred after primary fracturing was completed, creating more heterogeneity in the sampled data.

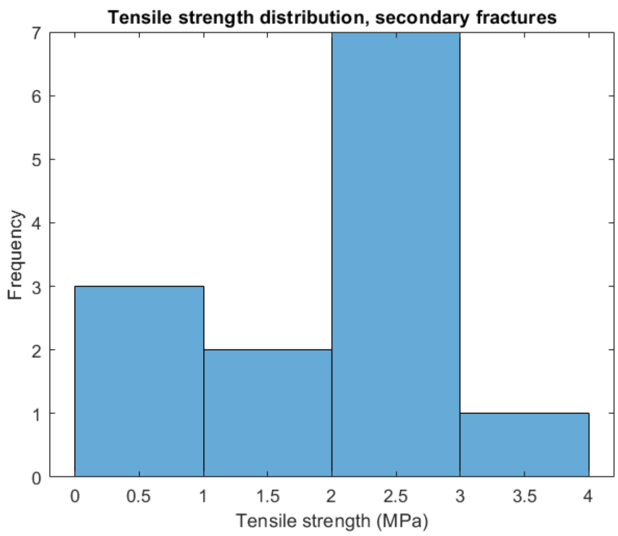

Figure 41: Histogram of secondary fracture tests

Table *8* shows each sample and its orientation under which the test was performed. The third column indicates to which case the result conforms. It shows that lower orientations tend to show results resembling case 1 & 2, while a larger relative orientation generally presents case 3 or 4.

Relative orientation	Sample	Case
20°	13	1
30°	4	1
30°	9	2
35°	11	4
37.5°	16	2
40°	6	3
45°	12	3
45°	14	4
50°	1	3
50°	7	4
60°	15	4
60°	20	4
90°	3	4

Table 8: Each sample and its behaviour

7.2.2 Zones

Based on the discussion from 7.2.1, it is proposed that four possible scenarios exist. The results from 6.2.1 show that depending on the angle between the original and new fracture different results can be expected. This is shown graphically in Figure 42. Here, mean values of tensile stress are plotted against the corresponding angle. A fitted line is drawn through these points. It clearly demonstrates that values between 60 and 90° are the highest, while tests performed between 20 and 40° are among the lowest. Generally, the closer the fractures are to being perpendicular, the higher the tensile strength. In contrast, the closer the fractures are to being parallel, the lower the tensile strength. In addition, the graph shows that there is no hard boundary for each case. The transitions between cases occur over a range, not a single degree.

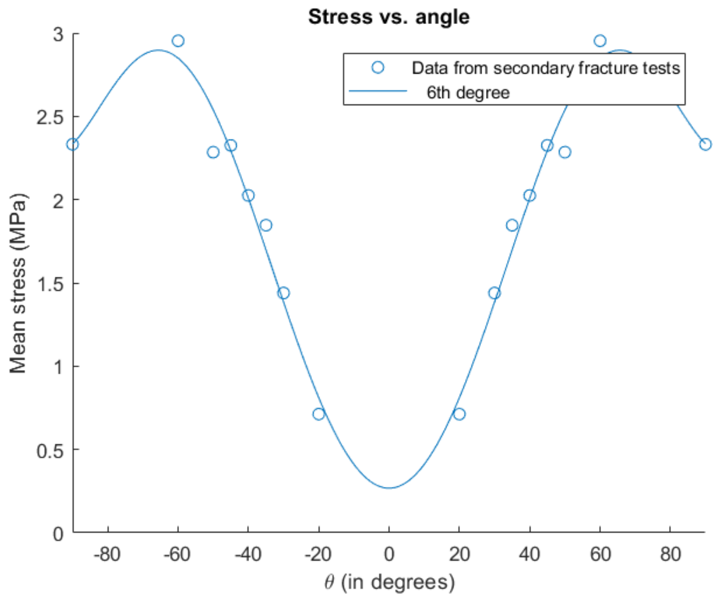

Figure 42: Stress against angle plot

The laboratory work and analysis of the results provide the suggested theory presented in Table 9. An important note to this table is that tests between 30-60° displayed both cases 2 and 3, although case 2 is more frequent in the lower region, and case 3 is more frequently seen in the upper parts. Therefore, Table 9 displays the typical behaviour as indicated by Section 6.2.1, but does not guarantee that this behaviour will occur.

Zone	Relative orientation	Typical behaviour	Tensile strength
Zone 1	0°-30°	Case 1: primary fracture does not close, no secondary fracture emerges, sliding occurs	Lowest
Zone 2	30°-45°	Case 2: primary fracture does not compact, secondary fractures form towards the end of the disk using a large part of the original fracture	Second lowest
Zone 3	45°-60°	Case 3: primary fracture closes slightly, secondary fracture forms using small, centre part of original fracture	Second highest
Zone 4	60°-90°	Case 4: primary fracture closes completely, secondary fracture forms independently of original fracture	Highest

Table 9: Suggested fracture zones and typical behaviour

In order to improve the theory presented in Table 9, it is advisable that more tests such as those in Section 6.2.1 are performed. This will allow for testing of the suggested theory and improve the accuracy of the orientations where typical behaviour is expected.

7.2.3 Fracture roughness

Figure 33 seems to indicate that secondary fractures are less rough at higher angles. However, results at 45° and 60° directly contradict this trend. Furthermore, the result at 40° is disproportionally high and likely not a trustworthy data point. This is most probably caused by a large deviation towards the bottom, as shown in Figure 43.

Figure 43: Secondary fracture at 40°

In addition to these discrepancies, the differences between the fracture roughness values are mostly relatively small. Therefore, the collected data on fracture roughness is not conclusive. In order to investigate if there is a trend where higher angles generate fewer rough fractures, more tests need to be performed at all angles.

8 Conclusion

The results presented in this thesis have shown that during the Brazilian Disc test, fractures form in the centre of the disk. This is because the stress concentration was demonstrated to be the highest at this location. The standard deviation and mean value of the tensile strength values were found to be in accordance with similar tests as analysed in literature, when compensated for a difference in porosity. During secondary fracture testing it was observed that under varying angles, four types of behaviour were displayed by the samples. Each of these four cases was found to be most common between certain ranges of rotation. It was suggested that four zones exist which individually dictate the typical behaviour seen after failure of the sample. These zones were suggested to be between 0° and 30°; 30° and 45°; 45° and 60° and finally 60° to 90°. It was noted that for cases where the original fracture closed, further research could investigate the impact of this on the permeability of the rock. Furthermore, analysis of the fracture roughness seemed to indicate that at angles closer to 90°, the roughness of the secondary fracture is less than the primary fracture. This seemed to occur in reverse at angles approaching 0°. However, notable exceptions and limited data led to the conclusion that the results from fracture roughness analysation are inconclusive. In order to provide more conclusive results, more secondary fracture tests should be performed and analysed on their fracture propagation and fracture roughness.

9 References

Andrews, E. (2018, August 22). *10 Surprising Facts About the Empire State Building*. Retrieved from History.com: https://www.history.com/news/10-surprising-facts-about-the-empire-state-building

Baykasoğlu, A., Güllü, H., Çanakçı, H., & Özbakır, L. (2008). Prediction of compressive and tensile strength of limestone via genetic programming. *Expert Systems with Applications, 35*(1-2), 111-123. Retrieved from http://www.sciencedirect.com/science/article/pii/S0957417407002163

Daneshy, A. (2010). *Hydraulic Fracturing to Improve Production.* SPE.

Einstein, H. H., & Dershowitz, W. S. (1990). Tensile and shear fracturing in predominantly compressive stress fields - a review. *Engineering Geology*(29), 149-172.

Kourkoulis, S. K., Markides, C. F., & Chatzistergos, P. E. (2013). The standardized Brazilian disc test as a contact problem. *International Journal of Rock Mechanics & Mining Sciences*(57), 132-141.

Li, D., & Wong, L. N. (2012, March). The Brazilian Disc Test for Rock Mechanics Applications: Review and New Insights. *Rock Mechanics and Rock Engineering*, 269-284.

Mellor, M., & Hawkes, I. (1971). Measurement of Tensile Strength by Diametral Compression of Discs and Annuli. *Engineering Geology*(5), 173-225.

Nazir, R., Momeni, E., Armaghani, D. J., & Amin, M. F. (2013). Correlation Between Unconfined Compressive Strength and Indirect Tensile Strength of Limestone Rock Samples. *EJGE, 18*(1), 1737-1746.

Perras, M., & Diederichs, M. (2014). A Review of the Tensile Strength of Rock: Concepts and Testing. *Geotechnical and Geological Engineering*(32), 525-546.

Powell, W. G. (2004). *Indiana Limestone*. Retrieved from academic.brooklyn.cuny.edu: http://academic.brooklyn.cuny.edu/geology/powell/613webpage/NYCbuilding/IndianaLimestone/IndianaLimestone.htm

Riera, J. D., Miguel, L. F., & Iturrioz, I. (2014). Assesement of Brazilian tensile test by means of the truss-like Discrete Element Method (DEM) with imperfect mesh. *Engineering Structures*(81), 10-21.

Rinehart, A. J., Bishop, J. E., & Dewers, T. (2015). Fracture propagation in Indiana Limestone interpreted via linear softening cohesive fracture model. *Solid Earth*(120), 2292-2308.

Schmidt, R. A. (1976). Fracture-toughness testing of limestone. *Experimental mechanics*(16), 161-167.

Selvadurai, P. A. (2010). *Permeability of Indiana Limestone: Experiments and Theoretical Concepts for Interpretation of Results.* Master Thesis, McGill University, Civil Engineering and Applied Mechanics, Montréal.

APPENDIX

I. Stress against time plots (primary fractures)

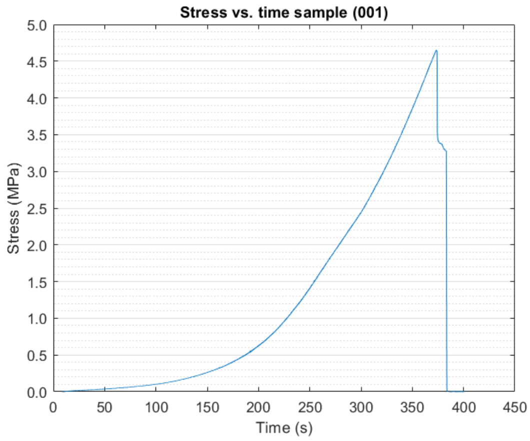

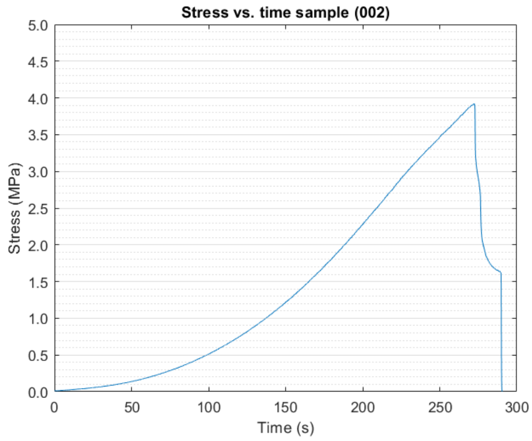

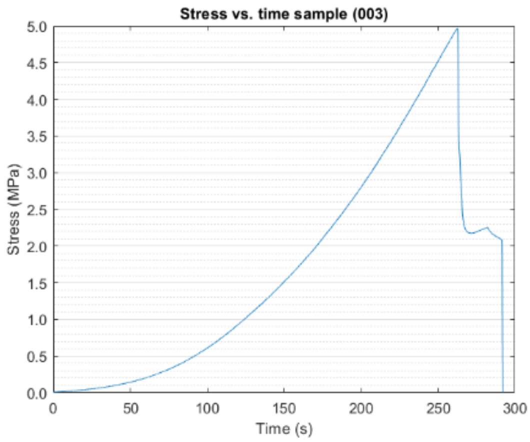

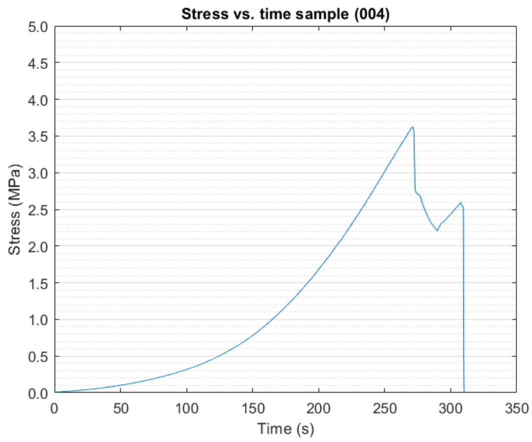

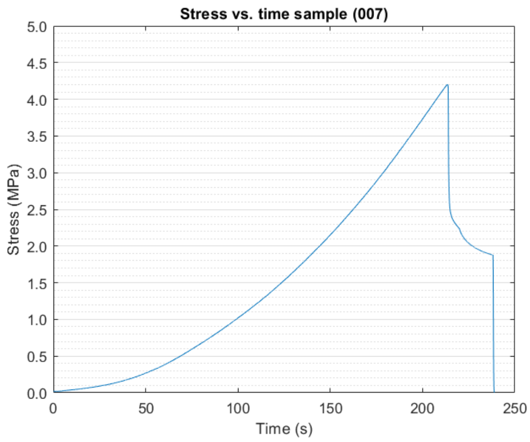

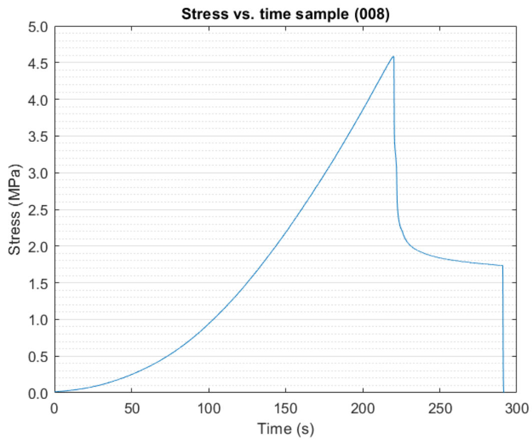

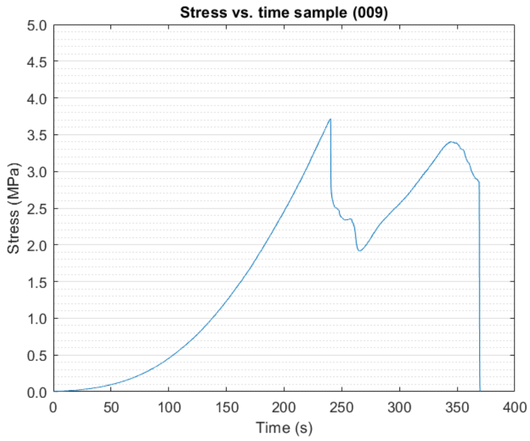

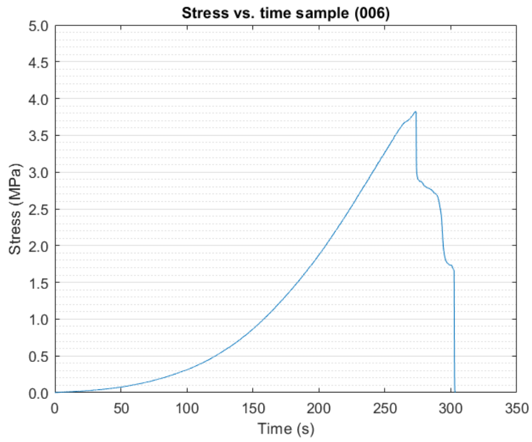

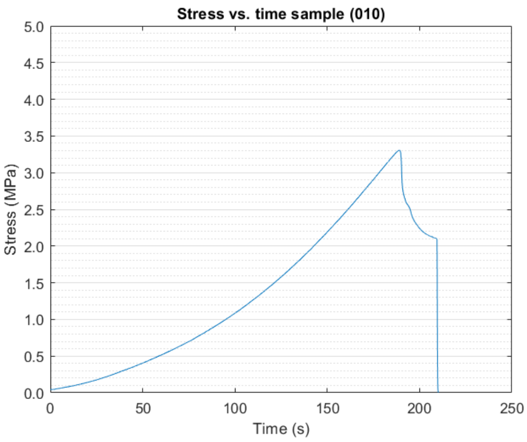
Stress vs. time sample (010)
Stress (MPa)
Time (s)

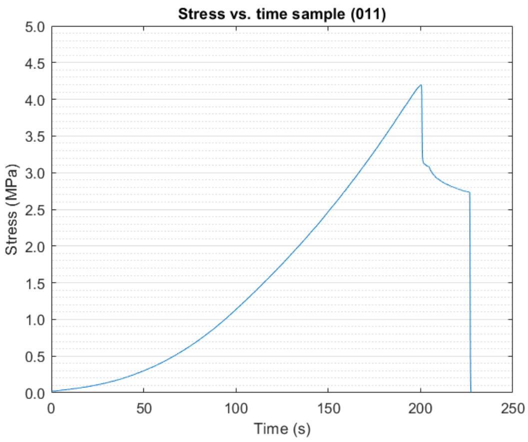
Stress vs. time sample (011)
Stress (MPa)
Time (s)

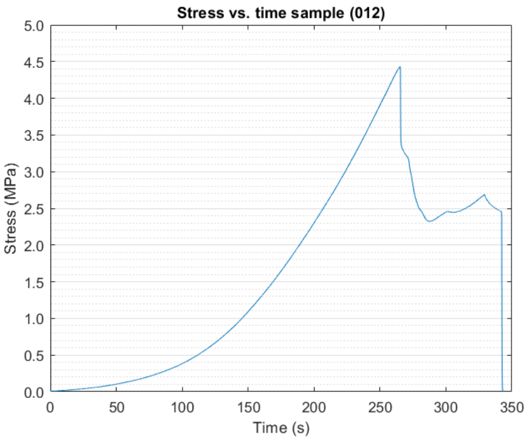
Stress vs. time sample (012)
Stress (MPa)
Time (s)

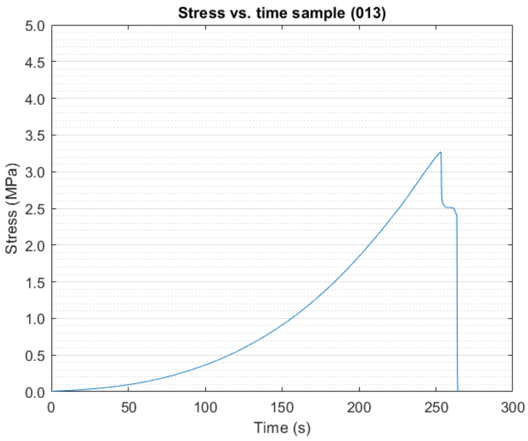
Stress vs. time sample (013)
Stress (MPa)
Time (s)

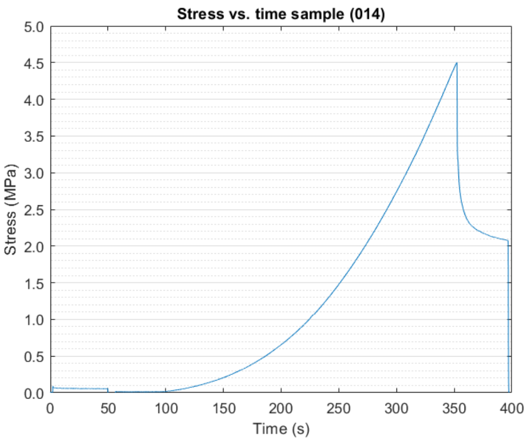
Stress vs. time sample (014)
Stress (MPa)
Time (s)

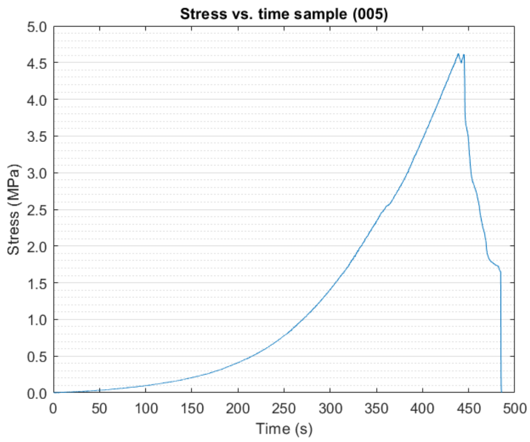
Stress vs. time sample (005)
Stress (MPa)
Time (s)

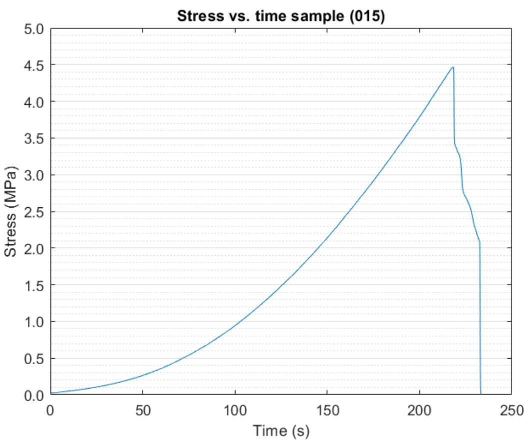
Stress vs. time sample (015)
Stress (MPa)
Time (s)

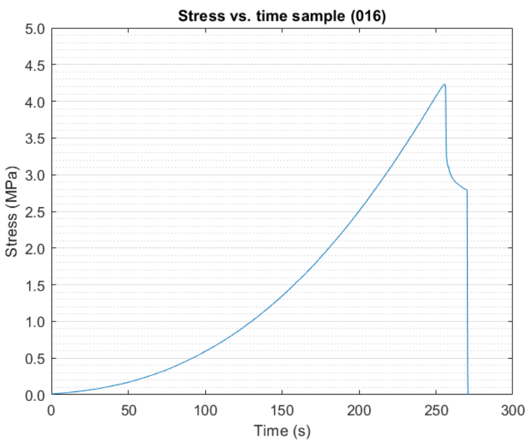
Stress vs. time sample (016)
Stress (MPa)
Time (s)

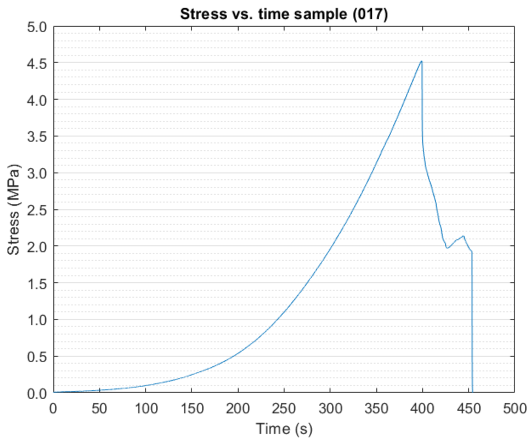
Stress vs. time sample (017)
Stress (MPa)
Time (s)
0.0
0.5
1.0
1.5
2.0
2.5
3.0
3.5
4.0
4.5
5.0
0
50
100
150
200
250
300
350
400
450
500

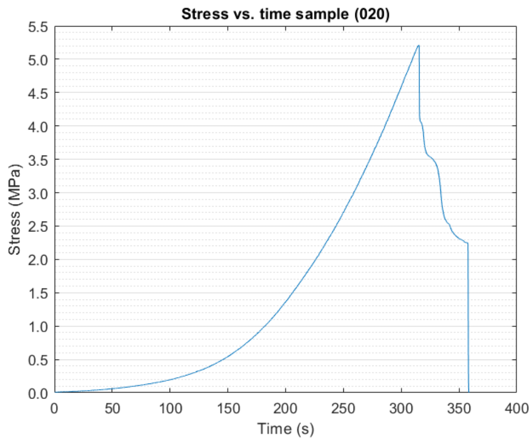
Stress vs. time sample (020)
Stress (MPa)
Time (s)
0.0
0.5
1.0
1.5
2.0
2.5
3.0
3.5
4.0
4.5
5.0
5.5
0
50
100
150
200
250
300
350
400

II. Stress against time plots (secondary fractures)

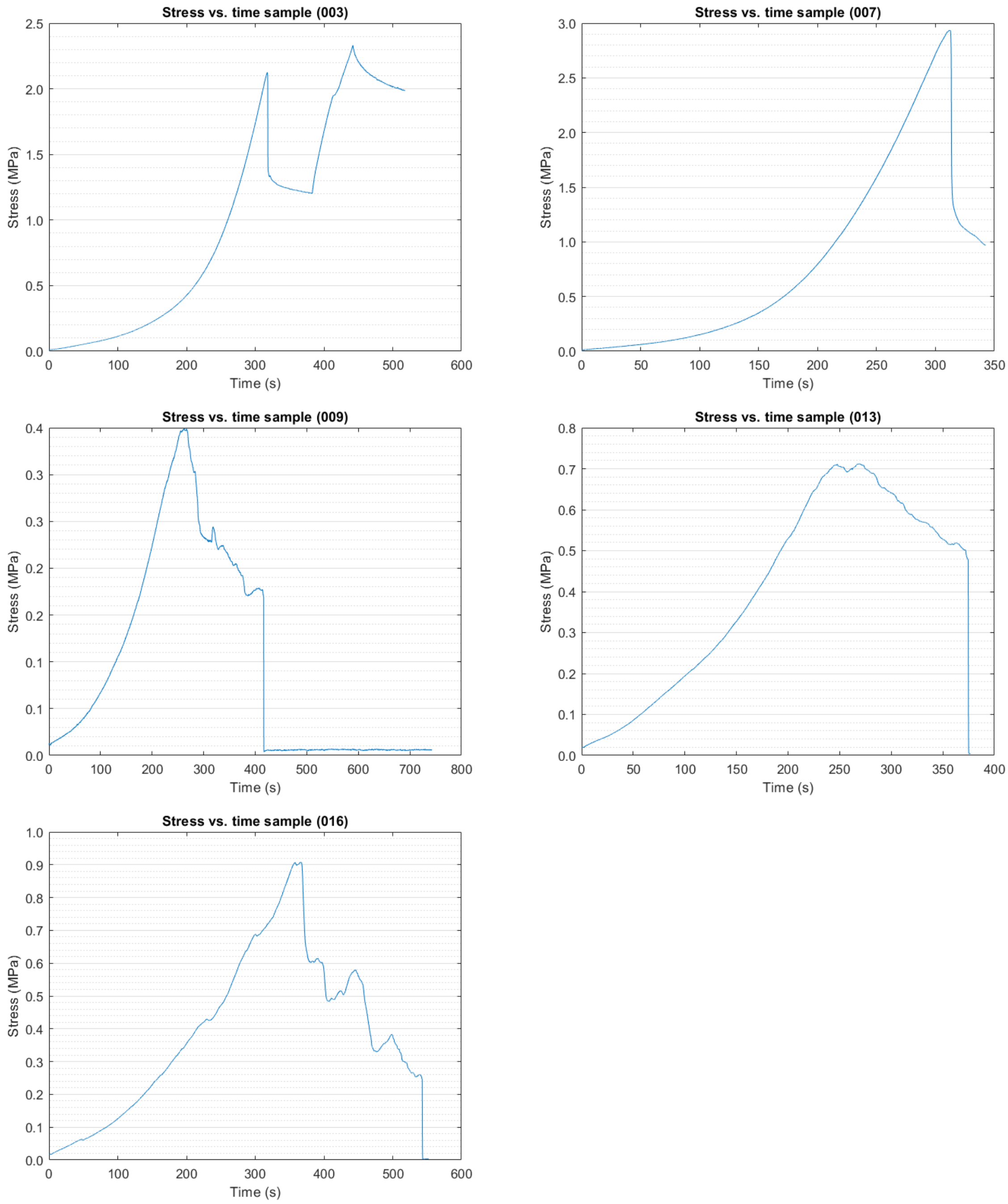

Figure 1: Stress against time plots (second batch)

III. Secondary fracture images

The images below depict the sample at the start of the second test; just before failure and after failure (from left to right).

20° - sample 13

30° - sample 4

30° - sample 9

35° - sample 11

37.5° - sample 16

40° - sample 6

45° - sample 12

45° - sample 14

50° - sample 1

50° - sample 007

60° - sample 15

60° - sample 20

90° - sample 3

IV. Fracture roughness images

The images show the drawn fractures used for the calculation of fracture roughness using Matlab. To the left, the primary fracture, to the left the secondary fracture. Note that not all samples are displayed as in two cases no secondary fracture was created.

30° - sample 9

35° - sample 11

37.5° - sample 16

40° - sample 6

45° - sample 12

45° - sample 14

50° - sample 1

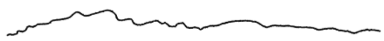

50° - sample 7

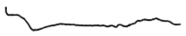

60° - sample 15

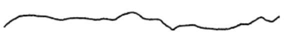

60° - sample 20

90° - sample 3

V. Fracture roughness – Matlab code

```
% Determine fracture roughness; by Anne Pluymakers, Auke Barnhoorn & Friso
% ter Steege

% read image data

clear
close all

A=imread('90_003_3.png');
%B=A(:,:,3);

grayImage = rgb2gray(A);
B = grayImage ~= 255;
% all three final bits of matrix show the same - if you want to image use:
% imshow(A)

% find the zero elements
[y,x]=find(B);

% interpreted line
figure
imagesc(B)

% for viewing:
figure
scatter(x,y,'.');

% for rms orientation of axes is important, not for peak2peak
c = polyfit(x,y,1);

% Display evaluated equation y = m*x + b
%disp(['Equation is y = ' num2str(c(1)) '*x + ' num2str(c(2))])

% Evaluate fit equation using polyval
y_est = polyval(c,x);
figure;
hold on
plot(x,y_est)
hold off

% bring points to zero
yzero(1:length(y),1)=zeros;
for i=1:length(y)
    yzero(i)=y(i)-c(:,2);
end

% you can't lose inclination without changing statistics of the signal
% when using simple parameter of rms or peak2peak. So let's just leave it
% like this

rough1=rms(yzero)

%rough2=peak2peak(yzero)

%% Plot bar graph
yy=[22.438 41.555; 22.960 37.647; 8.654 11.556; 7.314 81.398; 18.260 11.693; 9.334 40.709;
20.141 15.663; 16.839 14.722; 23.787 13.372; 24.000 27.257; 33.360 27.834];
bar(yy)
legend('Primary fracture', 'Secondary fracture')
xticklabels({'30\circ' '35\circ' '37.5\circ' '40\circ' '45\circ' '45\circ' '50\circ' '50\circ'
'60\circ' '60\circ' '90\circ'  })
ylabel('Rougness (measured in RMS)')
xlabel('Second fracture orientation')
title('Primary fracture roughness vs. secondary fracture roughness')
```

VI. Matlab code

```
% BEP Friso ter Steege

clear
close all
Lab1=xlsread('BEP-excel.xlsx');

%% Import data
Lab1=Lab1(5:end,:);
sample_no=Lab1(:,1);
weight=Lab1(:,5); %mm
length=Lab1(:,9); %mm
width=Lab1(:,13); %mm
bulk_volume=Lab1(:,14); %cm3
density=Lab1(:,15); %g/cm3
porosity_expected=Lab1(:,17);
matrix_volume=Lab1(:,18); %cm3
matrix_density=Lab1(:,19); %g/cm3
porosity=Lab1(:,20);
permeability=Lab1(:,21); %mD

%% Create figures
figure
H=histogram(porosity);
ylabel('Frequency')
xlabel('Porosity')
title('Histogram of measured porosities')

figure
scatter(sample_no,porosity_expected,'filled
')
hold on
scatter(sample_no,porosity,'filled')
hold on
scatter(sample_no,porosity-
porosity_expected,'filled')
hold off
legend('Expected porosity','Measured
porosity','Difference')
ylabel('Porosity')
xlabel('Sample number')
ylim([0 0.25])
xlim([1 22])
title('Expected porosity v.s. measured
porosity')
%differences due to mineral content &
chipping

figure
scatter(porosity_expected,density,'filled')
%hold on
%FO1 = fit(porosity_expected,density,
'poly1');
%plot(FO1)
%hold off
title('Density v.s. expected porosity')
ylabel('Density (g/cm^3)')
xlabel('Porosity')
legend('Density v.s. porosity')

figure
scatter(porosity,density,'filled')
hold on
%FO2 = fit(porosity,density, 'poly1');
%plot(FO2)
%hold off
title('Density v.s. measured porosity')
ylabel('Density (g/cm^3)')
xlabel('Porosity')
legend('Density v.s. porosity')

%% Part 2 - import data
data1=xlsread('data1.xlsx');
data2=xlsread('data2.xlsx');
data3=xlsread('data3.xlsx');
mean1=mean(data1(:,2));
std1=std(data1(:,2));
mean2=mean(data2(:,2));
std2=std(data2(:,2));
mean3=mean(data3(:,2));
std3=std(data3(:,2));
mean4=6.0;
std4=0.378;
mean5=3.8;
std5=2.5;
%1&5 are not Indiana Limestone, 2-4 are
Indiane Limestone
%% Errorbar plot
figure
errorbar(1,mean1,std1,'LineStyle','none','M
arker','x');
hold on
errorbar(2,mean2,std2,'LineStyle','none','M
arker','x');
hold on
errorbar(3,mean3,std3,'LineStyle','none','M
arker','x');
hold on
errorbar(4,mean4,std4,'LineStyle','none','M
arker','x');
hold on
errorbar(5,mean5,std5,'LineStyle','none','M
arker','x');
hold off
xlim([0 6])
xticklabels({'' 'Nazir et al. (2013)'
'Schmidt (1976)' 'Rinehart et al. (2015)'
'Mellow & Hawkes (1971)' 'Baykaso\circlu et
al. (2008)' ''  })
xlabel('Data source')
ylabel('Tensile strength (MPa)')
title('Tensile strength comparison')
ytickformat('%.1f')
ax = gca;
ax.YGrid = 'on';
ax.YMinorGrid = 'on';


%% -------------First tensile tests--------
------------------------------------------
---------
Lab2=xlsread('BEP-excel.xlsx');
Lab2=Lab2(5:end,:);
weight=Lab2(:,5); %g
D=Lab2(:,9); %mm
t=Lab2(:,13); %mm

%% Read data
A001=xlsread('FrisoterSteege_001.xlsx');
A002=xlsread('FrisoterSteege_002.xlsx');
A003=xlsread('FrisoterSteege_003.xlsx');
A004=xlsread('FrisoterSteege_004.xlsx');
A005=xlsread('FrisoterSteege_005.xlsx');
A006=xlsread('FrisoterSteege_006.xlsx');
A007=xlsread('FrisoterSteege_007.xlsx');
A008=xlsread('FrisoterSteege_008.xlsx');
A009=xlsread('FrisoterSteege_009.xlsx');
A010=xlsread('FrisoterSteege_010.xlsx');
A011=xlsread('FrisoterSteege_011.xlsx');
A012=xlsread('FrisoterSteege_012.xlsx');
A013=xlsread('FrisoterSteege_013.xlsx');
A014=xlsread('FrisoterSteege_014.xlsx');
A015=xlsread('FrisoterSteege_015.xlsx');
A016=xlsread('FrisoterSteege_016.xlsx');
A017=xlsread('FrisoterSteege_017.xlsx');
```

```
A020=xlsread('FrisoterSteege_020.xlsx');

%% Calculate MPa
A001(:,10)=(0.636*((A001(:,5)*1000)/(D(001,
:)*t(001,:))));
A002(:,10)=(0.636*((A002(:,5)*1000)/(D(002,
:)*t(002,:))));
A003(:,10)=(0.636*((A003(:,5)*1000)/(D(003,
:)*t(003,:))));
A004(:,10)=(0.636*((A004(:,5)*1000)/(D(004,
:)*t(004,:))));
A005(:,10)=(0.636*((A005(:,5)*1000)/(D(005,
:)*t(005,:))));
A006(:,10)=(0.636*((A006(:,5)*1000)/(D(006,
:)*t(006,:))));
A007(:,10)=(0.636*((A007(:,5)*1000)/(D(007,
:)*t(007,:))));
A008(:,10)=(0.636*((A008(:,5)*1000)/(D(008,
:)*t(008,:))));
A009(:,10)=(0.636*((A009(:,5)*1000)/(D(009,
:)*t(009,:))));
A010(:,10)=(0.636*((A010(:,5)*1000)/(D(010,
:)*t(010,:))));
A011(:,10)=(0.636*((A011(:,5)*1000)/(D(011,
:)*t(011,:))));
A012(:,10)=(0.636*((A012(:,5)*1000)/(D(012,
:)*t(012,:))));
A013(:,10)=(0.636*((A013(:,5)*1000)/(D(013,
:)*t(013,:))));
A014(:,10)=(0.636*((A014(:,5)*1000)/(D(014,
:)*t(014,:))));
A015(:,10)=(0.636*((A015(:,5)*1000)/(D(015,
:)*t(015,:))));
A016(:,10)=(0.636*((A016(:,5)*1000)/(D(016,
:)*t(016,:))));
A017(:,10)=(0.636*((A017(:,5)*1000)/(D(017,
:)*t(017,:))));
A020(:,10)=(0.636*((A020(:,5)*1000)/(D(020,
:)*t(020,:))));

%% Calculate max values
[max_001,i_001]=max(A001(:,10));
[max_002,i_002]=max(A002(:,10));
[max_003,i_003]=max(A003(:,10));
[max_004,i_004]=max(A004(:,10));
[max_005,i_005]=max(A005(:,10));
[max_006,i_006]=max(A006(:,10));
[max_007,i_007]=max(A007(:,10));
[max_008,i_008]=max(A008(:,10));
[max_009,i_009]=max(A009(:,10));
[max_010,i_010]=max(A010(:,10));
[max_011,i_011]=max(A011(:,10));
[max_012,i_012]=max(A012(:,10));
[max_013,i_013]=max(A013(:,10));
[max_014,i_014]=max(A014(:,10));
[max_015,i_015]=max(A015(:,10));
[max_016,i_016]=max(A016(:,10));
[max_017,i_017]=max(A017(:,10));
[max_020,i_020]=max(A020(:,10));

%% Calculate strain
for i = 1:4010
A001(i,11)=(A001(i+1,7)-
A001(1,7))./length(1);
end
for i = 1:3063
A002(i,11)=(A002(i+1,7)-
A002(1,7))./length(2);
end
for i = 1:3270
A003(i,11)=(A003(i+1,7)-
A003(1,7))./length(3);
end
for i = 1:3348
A004(i,11)=(A004(i+1,7)-
A004(1,7))./length(4);
end
for i = 1:4902
A005(i,11)=(A005(i+1,7)-
A005(1,7))./length(5);
end
for i = 1:3058
A006(i,11)=(A006(i+1,7)-
A006(1,7))./length(6);
end
for i = 1:2544
A007(i,11)=(A007(i+1,7)-
A007(1,7))./length(7);
end
for i = 1:3008
A008(i,11)=(A008(i+1,7)-
A008(1,7))./length(8);
end
for i = 1:3700
A009(i,11)=(A009(i+1,7)-
A009(1,7))./length(9);
end
for i = 1:2113
A010(i,11)=(A010(i+1,7)-
A010(1,7))./length(10);
end
for i = 1:2370
A011(i,11)=(A011(i+1,7)-
A011(1,7))./length(11);
end
for i = 1:3452
A012(i,11)=(A012(i+1,7)-
A012(1,7))./length(12);
end
for i = 1:2669
A013(i,11)=(A013(i+1,7)-
A013(1,7))./length(13);
end
for i = 1:4008
A014(i,11)=(A014(i+1,7)-
A014(1,7))./length(14);
end
for i = 1:2396
A015(i,11)=(A015(i+1,7)-
A015(1,7))./length(15);
end
for i = 1:2737
A016(i,11)=(A016(i+1,7)-
A016(1,7))./length(16);
end
for i = 1:4568
A017(i,11)=(A017(i+1,7)-
A017(1,7))./length(17);
end
for i = 1:3612
A020(i,11)=(A020(i+1,7)-
A020(1,7))./length(20);
end


%% Calculate tensile strength + plot each
sample
figure
plot(A001(1:(i_001+10),11),A001(1:(i_001+10
),10));
hold on
plot(A002(1:(i_002+10),11),A002(1:(i_002+10
),10));
hold on
plot(A003(1:(i_003+10),11),A003(1:(i_003+10
),10));
hold on
plot(A004(1:(i_004+10),11),A004(1:(i_004+10
),10));
hold on
plot(A005(1:(i_005+10),11),A005(1:(i_005+10
),10));
hold on
```

```
plot(A006(1:(i_006+10),11),A006(1:(i_006+10
),10));
hold on
plot(A007(1:(i_007+10),11),A007(1:(i_007+10
),10));
hold on
plot(A008(1:(i_008+10),11),A008(1:(i_008+10
),10));
hold on
plot(A009(1:(i_009+10),11),A009(1:(i_009+10
),10));
hold on
plot(A010(1:(i_010+10),11),A010(1:(i_010+10
),10));
hold on
plot(A011(1:(i_011+10),11),A011(1:(i_011+10
),10));
hold on
plot(A012(1:(i_012+10),11),A012(1:(i_012+10
),10));
hold on
plot(A013(1:(i_013+10),11),A013(1:(i_013+10
),10));
hold on
plot(A014(1:(i_014+10),11),A014(1:(i_014+10
),10));
hold on
plot(A015(1:(i_015+10),11),A015(1:(i_015+10
),10));
hold on
plot(A016(1:(i_016+10),11),A016(1:(i_016+10
),10));
hold on
plot(A017(1:(i_017+10),11),A017(1:(i_017+10
),10));
hold on
plot(A020(1:(i_020+10),11),A020(1:(i_020+10
),10));
hold off
xlabel('Strain')
ylabel('Stress (MPa)')
title('Stress vs. strain curves')
ytickformat('%.1f')
ax = gca;
ax.YGrid = 'on';
ax.YMinorGrid = 'on';
ax.YLim = [0 5.2];
ax.XLim = [0 0.015];
legend('1','2','3','4','5','6','7','8','9',
'10','11','12','13','14','15','16','17','20
','Location','northwest')

%% Calculate parameters
tensile_strength=[max_001 max_002 max_003
max_004 max_005 max_006 max_007 max_008
max_009 max_010 max_011 max_012 max_013
max_014 max_015 max_016 max_017 max_020];
mean_ts = mean(tensile_strength)
median_ts = median(tensile_strength)
std_ts = std(tensile_strength)
min_ts = min(tensile_strength)
max_ts = max(tensile_strength)
figure
histogram(tensile_strength)
ylabel('Frequency')
xlabel('Tensile strength (MPa)')
title('Tensile strength distribution')

%% -------------2nd + 3rd test, with turns-
-------------------------------------------
------
B016=xlsread('FrisoterSteege_375_016.xlsx')
;
B003=xlsread('FrisoterSteege_90_003.xlsx');
B007=xlsread('FrisoterSteege_50_007.xlsx');
B009=xlsread('FrisoterSteege_30_009.xlsx');
B013=xlsread('FrisoterSteege_20_013.xlsx');

%Follwing are 3rd test
B004=xlsread('FrisoterSteege_30_004.xlsx');
B011=xlsread('FrisoterSteege_35_011.xlsx');
B006=xlsread('FrisoterSteege_40_006.xlsx');
B014=xlsread('FrisoterSteege_45_014.xlsx');
B012=xlsread('FrisoterSteege_45_012.xlsx');
B001=xlsread('FrisoterSteege_50_001.xlsx');
B015=xlsread('FrisoterSteege_60_015.xlsx');
B020=xlsread('FrisoterSteege_60_020.xlsx');

%% Calculate MPa

B016(:,10)=(0.636*((B016(:,5)*1000)/(D(0016
,:)*t(0016,:))));
B003(:,10)=(0.636*((B003(:,5)*1000)/(D(003,
:)*t(003,:))));
B007(:,10)=(0.636*((B007(:,5)*1000)/(D(007,
:)*t(007,:))));
B009(:,10)=(0.636*((B009(:,5)*1000)/(D(009,
:)*t(009,:))));
B013(:,10)=(0.636*((B013(:,5)*1000)/(D(013,
:)*t(013,:))));

%3rd test
B004(:,10)=(0.636*((B004(:,5)*1000)/(D(004,
:)*t(004,:))));
B011(:,10)=(0.636*((B011(:,5)*1000)/(D(011,
:)*t(011,:))));
B006(:,10)=(0.636*((B006(:,5)*1000)/(D(006,
:)*t(006,:))));
B014(:,10)=(0.636*((B014(:,5)*1000)/(D(014,
:)*t(014,:))));
B012(:,10)=(0.636*((B012(:,5)*1000)/(D(012,
:)*t(012,:))));
B001(:,10)=(0.636*((B001(:,5)*1000)/(D(001,
:)*t(001,:))));
B015(:,10)=(0.636*((B015(:,5)*1000)/(D(015,
:)*t(015,:))));
B020(:,10)=(0.636*((B020(:,5)*1000)/(D(020,
:)*t(020,:))));

%% Calc max
[maxb_016,ib_016]=max(B016(:,10));
[maxb_003,ib_003]=max(B003(:,10));
[maxb_007,ib_007]=max(B007(:,10));
[maxb_009,ib_009]=max(B009(:,10));
[maxb_013,ib_013]=max(B013(:,10));
[maxb_004,ib_004]=max(B004(:,10));
[maxb_011,ib_011]=max(B011(:,10));
[maxb_006,ib_006]=max(B006(:,10));
[maxb_014,ib_014]=max(B014(:,10));
[maxb_012,ib_012]=max(B012(:,10));
[maxb_001,ib_001]=max(B001(:,10));
[maxb_015,ib_015]=max(B015(:,10));
[maxb_020,ib_020]=max(B020(:,10));

%% Calculate strain
for i = 1:max(size(B001))-1
B001(i,11)=(B001(i+1,7)-
B001(1,7))./length(1);
end
for i = 1:max(size(B003))-1
B003(i,11)=(B003(i+1,7)-
B003(1,7))./length(3);
end
for i = 1:max(size(B004))-1
B004(i,11)=(B004(i+1,7)-
B004(1,7))./length(4);
end
for i = 1:max(size(B006))-1
B006(i,11)=(B006(i+1,7)-
B006(1,7))./length(6);
end
for i = 1:max(size(B007))-1
B007(i,11)=(B007(i+1,7)-
B007(1,7))./length(7);
```

```
end
for i = 1:max(size(B009))-1
B009(i,11)=(B009(i+1,7)-
B009(1,7))./length(9);
end
for i = 1:max(size(B011))-1
B011(i,11)=(B011(i+1,7)-
B011(1,7))./length(11);
end
for i = 1:max(size(B012))-1
B012(i,11)=(B012(i+1,7)-
B012(1,7))./length(12);
end
for i = 1:max(size(B013))-1
B013(i,11)=(B013(i+1,7)-
B013(1,7))./length(13);
end
for i = 1:max(size(B014))-1
B014(i,11)=(B014(i+1,7)-
B014(1,7))./length(14);
end
for i = 1:max(size(B015))-1
B015(i,11)=(B015(i+1,7)-
B015(1,7))./length(15);
end
for i = 1:max(size(B016))-1
B016(i,11)=(B016(i+1,7)-
B016(1,7))./length(16);
end
for i = 1:max(size(B020))-1
B020(i,11)=(B020(i+1,7)-
B020(1,7))./length(20);
end

%% Calculate stress strain curves
figure
plot(B015(1:(ib_015+30),11),B015(1:(ib_015+
30),10));
hold on
plot(B020(1:(ib_020+30),11),B020(1:(ib_020+
30),10));
hold on
plot(B003(1:(ib_003+30),11),B003(1:(ib_003+
30),10));
hold off
xlabel('Strain')
ylabel('Stress (MPa)')
title('Secondary fracture: stress vs.
strain curves')
ytickformat('%.1f')
ax = gca;
ax.YGrid = 'on';
ax.YMinorGrid = 'on';
ax.YLim = [0 3.2];
ax.XLim = [0 0.016];
legend('60\circ; sample 15','60\circ;
sample 20','90\circ; sample
3','Location','northwest')

figure
plot(B013(1:(ib_013+30),11),B013(1:(ib_013+
30),10));
hold on
plot(B004(1:(ib_004+30),11),B004(1:(ib_004+
30),10));
hold on
plot(B009(1:(ib_009+30),11),B009(1:(ib_009+
30),10));
hold on
plot(B011(1:(ib_011+30),11),B011(1:(ib_011+
30),10));
hold on
plot(B016(1:(ib_016+30),11),B016(1:(ib_016+
30),10));
hold off
xlabel('Strain')
ylabel('Stress (MPa)')
title('Secondary fracture: stress vs.
strain curves')
ytickformat('%.1f')
ax = gca;
ax.YGrid = 'on';
ax.YMinorGrid = 'on';
ax.YLim = [0 3.2];
ax.XLim = [0 0.015];
legend('20\circ; sample 13','30\circ;
sample 4','30\circ; sample 9','35\circ;
sample 11','37.5\circ; sample
16','Location','northwest')

figure
plot(B006(1:(ib_006+30),11),B006(1:(ib_006+
30),10));
hold on
plot(B012(1:(ib_012+30),11),B012(1:(ib_012+
30),10));
hold on
plot(B014(1:(ib_014+30),11),B014(1:(ib_014+
30),10));
hold on
plot(B007(1:(ib_007+30),11),B007(1:(ib_007+
30),10));
hold on
plot(B001(1:(ib_001+30),11),B001(1:(ib_001+
30),10));
hold off
xlabel('Strain')
ylabel('Stress (MPa)')
title('Secondary fracture: stress vs.
strain curves')
ytickformat('%.1f')
ax = gca;
ax.YGrid = 'on';
ax.YMinorGrid = 'on';
ax.YLim = [0 3.2];
ax.XLim = [0 0.015];
legend('40\circ; sample 6','45\circ; sample
12','45\circ; sample 14','50\circ; sample
7','50\circ; sample
1','Location','northwest')

%% Theta plot
xvector=[20 30 35 40 45 50 60 90];
yvector=[maxb_013 mean([maxb_004 maxb_009])
mean([maxb_011 maxb_016]) maxb_006
mean([maxb_012 maxb_014]) mean([maxb_007
maxb_001]) maxb_015 maxb_003];
xvector2=[-20 -30 -35 -40 -45 -50 -60 -90];
xvector3=[xvector2 xvector];
yvector3=[yvector yvector];

scatter(xvector3, yvector3)
ax = gca;
ax.YLim = [0 3];
ax.XLim = [-90 90];
legend('Data from secondary fracture
tests')
xlabel('\theta (in degrees)')
ylabel('Mean stress (MPa)')
title('Stress vs. angle')

%% Calc parameters
%B_tensile_strength=[maxb_003 maxb_007
maxb_009 maxb_013 maxb_016];
%B_mean_ts = mean(B_tensile_strength)
%B_median_ts = median(B_tensile_strength)
%B_std_ts = std(B_tensile_strength)
%B_min_ts = min(B_tensile_strength)
%B_max_ts = max(B_tensile_strength)
```